UNIVERSIDADE FEDERAL DE MINAS GERAIS
Instituto de Ciências Biológicas
Programa de Pós-graduação em Biologia Celular

Igor Barbosa Lima

Using of phosphate nanocomposites for therapeutics in melanoma model

Belo Horizonte
2021

Igor Barbosa Lima

Using of phosphate nanocomposites for therapeutics in melanoma model

Versão final

Tese apresentada ao programa de Pós-graduação em Biologia Celular da Universidade Federal de Minas Gerais como requisite parcial para obtenção do título de Doutor em Biologia Celular.

Orientadora: Dr. Fernanda R.C.L. de Almeida

Belo Horizonte

2021

043 Lima, Igor Barbosa.
Using of phosphate nanocomposites for therapeutics in melanoma model in vitro [manuscrito] / Igor Barbosa Lima. – 2021.
72 f. : il. ; 29,5 cm.

Orientadora: Dr. Fernanda R.C.L. de Almeida.
Tese (doutorado) – Universidade Federal de Minas Gerais, Instituto de Ciências Biológicas. Programa de Pós-Graduação em Biologia Celular.

1. Biologia Celular. 2. Envelhecimento. 3. Cardiotoxicidade. 4. Quimioterapia. 5. Adsorção. I. Almeida, Fernanda Radicchi Campos Lobato de. II. Universidade Federal de Minas Gerais. Instituto de Ciências Biológicas. III. Título.

CDU: 576

Ficha catalográfica elaborada pela bibliotecária Fabiane C M Reis – CRB 6 – 2680

UNIVERSIDADE FEDERAL DE MINAS GERAIS
INSTITUTO DE CIÊNCIAS BIOLÓGICAS
PROGRAMA DE PÓS-GRADUAÇÃO EM BIOLOGIA CELULAR

ATA DA DEFESA DE TESE DE DOUTORADO DE IGOR BARBOSA LIMA

239/2021 _ ENTRADA 1º/2018 _ 2018697530

Às **quatorze horas** do dia **20 de setembro de 2021**, reuniu-se de modo remoto, na plataforma microsoft teams, a Comissão Examinadora da Tese, indicada pelo Colegiado do Programa, para julgar, em exame final, o trabalho final intitulado: **"USING OF PHOSPHATE NANOCOMPOSITES FOR THERAPEUTICS IN MELANOMA MODEL IN VITRO"**, requisito final para obtenção do grau de Doutor em Biologia Celular. Abrindo a sessão, o Presidente da Comissão, **Dra. Fernanda Radicchi C. L. de Almeida (Presidente)**, após dar a conhecer aos presentes o teor das Normas Regulamentares do Trabalho Final, passou a palavra ao candidato, para apresentação de seu trabalho. Seguiu-se a arguição pelos examinadores, com a respectiva defesa do candidato. Logo após, a Comissão se reuniu, sem a presença do candidato e do público, para julgamento e expedição de resultado final. Foram atribuídas as seguintes indicações:

Prof./Pesq.	**Instituição**
Dra. Fernanda Radicchi C. L. de Almeida (Presidente)	UFMG
Dr. Guilherme Mattos Jardim Costa	UFMG
Dra. Vanessa Pinho da Silva	UFMG
Dra. Mônica Morais Santos	UFV
Dra. Nayara Ingrid de Medeiros	Instituto René Rachou - Fiocruz/MG

Pelas indicações, o candidato foi considerado: APROVADO

O resultado final foi comunicado publicamente ao candidato pelo Presidente da Comissão. Nada mais havendo a tratar, o Presidente encerrou a reunião e lavrou a presente ATA, que será assinada por todos os membros participantes da Comissão Examinadora. **Belo Horizonte, 20 de setembro de 2021.**

Dra. Fernanda Radicchi C. L. de Almeida (Presidente)

Dr. Guilherme Mattos Jardim Costa

Drª. Vanessa Pinho da Silva

Drª. Mônica Morais Santos

Drª. Nayara Ingrid de Medeiros

Obs: Este documento não terá validade sem a assinatura do Coordenador

Documento assinado eletronicamente por **Guilherme Mattos Jardim Costa**, **Professor do Magistério Superior**, em 21/09/2021, às 14:10, conforme horário oficial de Brasília, com fundamento no art. 5º do Decreto nº 10.543, de 13 de novembro de 2020.

Documento assinado eletronicamente por **Vanessa Pinho da Silva**, **Professora do Magistério Superior**, em 21/09/2021, às 14:21, conforme horário oficial de Brasília, com fundamento no art. 5º do Decreto nº 10.543, de 13 de novembro de 2020.

Documento assinado eletronicamente por **Mônica Morais Santos**, **Usuário Externo**, em 22/09/2021, às 09:18, conforme horário oficial de Brasília, com fundamento no art. 5º do Decreto nº 10.543, de 13 de novembro de 2020.

Documento assinado eletronicamente por **Fernanda Radicchi Campos Lobato de Almeida**, **Professora do Magistério Superior**, em 22/09/2021, às 11:04, conforme horário oficial de Brasília, com fundamento no art. 5º do Decreto nº 10.543, de 13 de novembro de 2020.

Documento assinado eletronicamente por **Nayara Ingrid de Medeiros**, **Usuário Externo**, em 24/09/2021, às 17:43, conforme horário oficial de Brasília, com fundamento no art. 5º do Decreto nº 10.543, de 13 de novembro de 2020.

A autenticidade deste documento pode ser conferida no site https://sei.ufmg.br/sei/controlador_externo.php?acao=documento_conferir&id_orgao_acesso_externo=0, informando o código verificador **0975369** e o código CRC **7E74AD89**.

Referência: Processo nº 23072.249570/2021-91 SEI nº 0975369

DEDICATION

To all students who suffer moral harassment in graduate school, I dedicate.

EPIGRAPH

Life always finds a way…

Dr. Ian Malcon in Jurassic Park by Michael Crichton

RESUMO

As taxas de incidência de melanoma têm aumentado dramaticamente nos últimos anos. A busca por estratégias que aumentem a eficácia terapêutica e reduzam os efeitos colaterais é o foco de diversos estudos na atualidade. O tratamento utiliza principalmente drogas bloqueadoras da cinase BRAF, entretanto, vários estudos têm demonstrado a eficácia de outras drogas quimioterápicas, como a doxorrubicina e a cisplatina, no tratamento do melanoma, mas os efeitos colaterais são fatores limitantes. A associação de quimioterápicos com nanopartículas é uma alternativa viável para potencializar a quimioterapia tradicional, visando à redução dos efeitos colaterais. Neste estudo apresentamos duas abordagens: a primeira destinada a adsorver cisplatina em nanopartículas de fosfato de cálcio (NPC), bem como quantificar a cisplatina encapsulada na formulação 91OCis e avaliar sua eficiência como carreadores para a entrega de drogas às células de melanoma (A375 e B16F10), e prever a seletividade das formulações usando células HEK-293. As análises de TXRF mostraram que 91OCis encapsula 9,6 μg de cisplatina a cada 1 mg e que NPC não consegue adsorver cisplatina em sua superfície. As formulações não foram capazes de reduzir a viabilidade celular nas linhagens testadas, provavelmente porque a cisplatina não é liberada da estrutura das nanopartículas no caso do 91OCis. Por outro lado, o cloridrato de doxorrubicina foi associado a nanopartículas de fosfato de cálcio funcionalizadas com ácido hialurônico e polietilenoglicol e testado em um modelo de melanoma *humano in vitro* usando a linha celular A-375. As formulações testadas mostraram uma redução significativa na IC_{50} ao longo de 48 horas quando comparadas com a droga livre (Dox 0,44 ± 0,25; N-DOX 0,13 ± 0,07; NPC+DOX 0,16 ± 0,08 μM) e toxicidade reduzida em células HEK-293. A formulação proporcionou uma redução significativa no IC_{50} ao longo de 48 horas (0,142 ± 0,07) quando comparada ao fármaco livre (0,44 ± 0,25) e toxicidade reduzida em células HEK-293. Ambos os tratamentos causaram danos ao DNA, tetraploidia após 72 horas, aumento da área nuclear e aumento da atividade da beta-galactosidase associada à senescência. Além disso, não houve formação de colônias após 14 dias de incubação precedida por tratamento de curta exposição. Os resultados preliminares indicam que a doxorrubicina nano-formulada tem potencial para o tratamento do melanoma, uma vez que potencializa a atividade da doxorrubicina sem alterar o mecanismo de ação e não aumenta a toxicidade para mioblastos de rato da linhagem celular H9C2.

Palavras-chave: Senescência; previsão de segurança; cardiotoxicidade; scapers; adjuvante; adsorção; quimioterapia; nanoterapêutica.

ABSTRACT

The incidence rates of melanoma have been increasing dramatically in recent years. The search for strategies that increase therapeutic efficiency and reduce side effects is the focus of several studies today. The treatment mainly uses BRAF kinase blocking drugs, however, several studies have demonstrated the efficiency of other chemotherapeutic drugs such as doxorubicin and cisplatin to treat melanoma, but the side effects are limiting factors. The association of chemotherapeutic agents with nanoparticles is a viable alternative to enhance traditional chemotherapy, aiming at reducing side effects. In this study, we present two approaches: the first one intended to adsorb cisplatin on calcium phosphate nanoparticles (NPC), as well as quantify the encapsulated cisplatin in the 91OCis formulation and evaluate its efficiency as carriers for the delivery of drugs to melanoma cells (A375 and B16F10) and predict the selectivity of the formulations using HEK-293 cells. Total X-ray fluorescence spectroscopy (TXRF) analyzes showed that 91OCis encapsulates 9.6 μg of cisplatin every 1 mg and that NPC cannot adsorb cisplatin on its surface. The formulations were not able to reduce cell viability in the tested cell lines, probably because cisplatin is not released from the nanoparticle structure in the case of 91OCis. On the other hand, doxorubicin hydrochloride was associated with calcium phosphate nanoparticles functionalized with hyaluronic acid and polyethylene glycol and tested in a human melanoma model *in vitro* using the A-375 cell line. The formulations tested showed a significant reduction in IC_{50} over 48 hours when compared to the free drug (Dox 0.44 ± 0.25; N-DOX 0.13 ± 0.07; NPC+DOX 0.16 ± 0.08 μM) and reduced toxicity in HEK-293 cells. The formulation provided a significant reduction in IC_{50} over 48 hours (0.142 ± 0.07) when compared to the free drug (0.44 ± 0.25) and reduced toxicity in HEK-293 cells. Both treatments caused DNA damage, tetraploidy after 72 hours, an increase in the nuclear area, and increased activity of senescence-associated beta-galactosidase. Also, there was no formation of colonies after 14 days of incubation preceded by short exposure treatment. Preliminary results indicate that nano-formulated doxorubicin has potential for melanoma treatment since it potentializes doxorubicin activity without changing the mechanism of action and does not increase toxicity to rat myoblasts of the H9C2 cell line.

Keywords**:** Senesce; safety prediction; cardiotoxicity; scapers; adjuvant; adsorption; chemotherapy; nanotherapeutics.

ABBREVIATIONS

91OCis - calcium phosphate nanoparticles with encapsulated cisplatin

AO - acridine orange

AVO - acidic vesicular organelles

Ca - calcium

Ccis - concentração de cisplatina

Cis - Cisplatin

DCF-DA - 2′,7′-Dichlorofluorescin diacetate

DMSO - Dimethyl Sulfoxide

Dox - doxorubicin

EDTA - ethylenediamine tetra-acetic acid

FACS - fluorescence-activated cell sorting

FM - final mass

HA - hyaluronic acid

HFS - hypotonic fluorochromic solution

HPLC - high-performance liquid chromatography

IC_{50} - cytotoxic concentration for 50% of the population

IM - initial mass

Mg - magnesium

MN - N-DOX mass

N-Cis – nanocaried cisplatin

N-Dox^- - nanocaried doxorubicin non-functionalized

N-Dox – nanocaried doxorubicin functionalized

NII - nuclear irregularity index

NMA - nuclear morphometric analysis

NC - Number of colonies

NPC - functionalized calcium phosphate nanoparticles

NPC^- - non-functionalized calcium phosphate nanoparticle

NPC+DOX - physical mixture of doxorubicin and functionalized calcium phosphate nanoparticles

OD - optical density

P - phosphorus

P- pellet

PBS - phosphate-buffered saline

PE - plating efficiency

PEG - polyethylene glycol

PRE - permeability retention effect

Pt - platinum

ROS - oxigen-reactive species

S1 - supernatant 1

S2 – supernatant 2

S3 – supernatant 3

SA-β-Gal - senescence-associated β-galactosidase

SF - survival fraction

SI – selectivity index

SRB - 2-(3-diethylamino-6-diethylazaniumylidene-xanthen-9-yl)-5-sulfo-benzenesulfonate

TCA - trichloroacetic acid

TXRF - total X-ray fluorescence spectroscopy

X-Gal - 5-bromo-4-chloro-3-indoxyl-β-D-galactopyranoside

ζ - zeta potential

FIGURES

TABLES

SUMMARY

1. General introduction

Cancer remains a major public health problem around the world. In the U.S., the disease is the second leading cause of death, being second only to cardiovascular diseases (SIEGEL; MILLER; JEMAL, 2020). In Brazil, 600.000 new cases were reported for the 2018-2019 biennium (INCA, 2020). Thus, the prospect of new drugs and formulations that increase therapeutic efficiency is essential for the improvement of treatments that generate severe side effects, in addition to drug resistance (HANUSOVA et al., 2015).

Among the various types of skin cancer, melanoma is characterized by developing faster and being aggressive. Its occurrence has been increasing over the years. A prediction made by the American Cancer Society (ACS) informs that at least 76.100 new cases and 9.710 deaths from melanoma will be reported in the coming years (LARKIN et al., 2015). The highest incidence of melanoma occurs in men over the age of 65, however, in recent years the occurrence in women aged between 25 and 39 years has increased considerably (BASTIAN, 2014). There is no consensus on what the predominant risk factor for the development of melanoma is. It is known that intense and intermittent sun exposure is one of the main triggers, as well as genetic factors, exposure to certain chemicals, and immunosuppression (BERWICK et al., 2016). It is the less common type of skin cancer, but it is the most serious. In Brazil, it is estimated that in the period between 2018 and 2019, 6.260 new cases, and 2015 1.794 deaths caused by the disease were reported (INCA, 2020).

Melanoma develops from pigmented cells whereas non-melanoma skin cancer develops from unpigmented cells such as squamous cell basal cells. Approximately 60% of melanoma cases have a mutation that results in the overexpression of the B-raf proto-oncogene present at locus 24 of chromosome seven, concomitant with a reduction in the activity of the p53 enzyme (LARKIN et al., 2015).

This enzyme is important for cell cycle progression by initiating the signaling cascade that leads to normal cell proliferation and survival from an external stimulus (e.g. growth factors and hormones). However, when this gene is overexpressed, the cell accumulates BRAF units that trigger the signaling pathway without the need for external stimuli. leading cells proliferated uncontrollably. This pathway have become a tagert for

melanoma treatment with the development of drugs that act directly by blocking BRAF activity, reducing proliferation rates (SCHADENDORF et al., 2015).

Malignant tumors are usually associated with an unfavorable prognosis. The methods traditionally used in the treatment of neoplasms use surgical interventions, chemotherapy, and radiotherapy. Conventional chemotherapy has a series of unwanted effects, since the chemotherapeutic agent is distributed systemically and not selectively, causing damage to healthy cells (HALEY; FRENKEL, 2008). Thus, generating a demand for research for more efficient therapies aiming at minimization of side effects (SHEN et al., 2015).

Chemotherapy was the main therapeutic method used in advanced cases of melanoma. Currently, scientific studies have provided differentiated and integrated therapies, such as the association between traditional chemotherapy and immunotherapy. The use of chemotherapeutic agents associated with a high dose of interleukin-2 (IL-2) is still the strategy most frequently used in the treatment of advanced cases of melanoma. New treatment alternatives for melanoma have been tested in recent years, but little progress has been made (WILSON; SCHUCHTER, 2016)

Currently, the first-line treatment suggested for cases of BRAF+ melanoma is based on the use of BRAFq inhibitory drugs. During in vitro and preclinical trials, the use of BRAF inhibitor drugs has been shown to reduce the proliferative rate in cases conditioned to this mutation (SCHADENDORF et al., 2015).

Dabrafenib is the main chemotherapeutic agent used in the treatment of melanoma cases that have V600E or V600K mutations in the BRAF gene since it can inhibit the growth of cancerous cells (ASCIERTO et al., 2011). Tests carried out during phase 2 for the use of Dabrafenib® demonstrated that it is a tolerable drug and patients showed favorable responses to treatment (ASCIERTO et al., 2013). During phase 3, it was observed that this drug can improve the survival of patients, interrupting the progression of the tumor. However, the treatment has side effects such as skin toxicity, fever, fatigue, arthralgia, and headaches (HAUSCHILD et al., 2012). Also, several patients show resistance to treatment after six or nine months (LONG et al., 2014)

There are cases of melanoma in which this mutation is not present, bringing up a demand for the use of treatments focused on alternative therapeutic targets (HUTCHINSON et al., 2013). Among these we can cite platinum derivatives such as

Cisplatin (Cis). These drugs have been used for a long time to treat cancer but cause severe side effects during chemotherapy and mainly leave neurological and renal sequelae in the patient after use (FLOREA et al, 2011). Cisplatin's mechanism of action is based on the formation of adducts on the DNA strands. The binding causes damage to the DNA repair mechanism and leads to both cancerous and healthy cell death. Systemic distribution of the drug causes severe side effects (FUERTES et al., 2003).

Doxorubicin is another drug that has an efficient antiproliferative effect but also generates serious side effects during treatment (nausea, headache, etc.) and long-term sequelae (ABDULELA et al., 2021). The main sequelae are dose-dependent heart disease and nephropathy. In this context, the reduction of the effective dose becomes a therapeutic target of interest. Usually doxorubicin is not used as a treatment for melanoma cases due to side effects. When the diagnosis is made early, surgical removal of the tumor and adjacent tissues is chosen. This strategy is completely efficient but in advanced cases of melanoma metastasis development occurs rapidly (mainly in the lung) (XIAO et al.,2017).

Melanoma cases that are not conditioned to BRAF gene mutation need attention due to the occurrence of multiple drug resistance. The search for alternative, more efficient therapies that do not cause severe harm to patients is extremely important to prevent deaths and improve the quality of life of patients in advanced stage of melanoma (TANGELLA., 2021).

Nanoparticles are able to increase the specificity of drugs for tumors due to intrinsic characteristics of the tumor microenvironment, such as anomalous angiogenesis that develops irregular and tortuous blood vessels, in addition to acidic pH, and secretion of inflammatory cytokines. When nanoparticles pass through the circulation and enter the tumor vasculature, there is a tendency for them to be trapped in this tangle of blood vessels and accumulate in the tumor (HUANG et al., 2021).

In this context of searching for new therapeutic strategies, the use of nanoparticles in drug delivery systems to specific sites of the tissues affected by tumors is a widely used methodology. It allows the chemotherapeutic agent to reach the target in an optimized way, providing a higher therapeutic index (FAHMY et al., 2005). For example, the application of gold nanoparticles conjugated to doxorubicin enhanced its effectiveness to treat melanoma in a murine model (ZHANG; TEODORO; NADEAU, 2015).

Controlled drug delivery to specific tissue sites affected by the tumor is a desirable strategy to optimize its pharmacological action (BAE; PARK, 2011). Structured nanoparticles function as efficient vehicles in delivering chemotherapeutic agents to specific affected locations (RUENRAROENGSAK; COOK; FLORENCE, 2010). This feature allows them to be used for the development of more efficient therapeutic methods and with reduced side effects (HOFFMAN, 2008).

The use of nanoparticles in the delivery of drugs to specific sites of the tissues affected by tumors has been a strategy widely used since it allows the chemotherapeutic agent to reach the target in an optimized way, providing a higher therapeutic index and overcoming physiological barriers (PINAR et al., 2021).

The association of Dox with calcium phosphate nanoparticles (NPC) has the potential to develop a new therapeutic strategy with reduced side effects compared to the free drug. However, the possibility of being used as an efficient therapeutic platform for the treatment of human melanoma has not yet been investigated. In this context, this work aims to test the effectiveness of two formulations (one named N-Dox and another named NPC+DOX) based on NPC. The formulations were tested against mammary tumor cells and MDA-MB231 and it was observed that even those nanoparticles containing a significantly lower concentration of doxorubicin, the treatment was able to reduce cell viability (TÓTARO, 2017). Based on our previous results, we hypothesized that calcium phosphate nanoparticles loaded with doxorubicin

This strategy aims to potentiate the effect of Dox against the human melanoma cell line A-375, as well as to reduce its toxicity. The physical-chemical characterization of the functionalized nanoparticles was carried out and to measure their *in vitro* efficacy, cytotoxicity assays were performed with human melanoma cells and non-tumor cells. Also evaluated their effect on cell clonogenic survival, as well as the investigation of the mechanism of cytotoxicity through flow cytometry.

2. General objectives

This work session aimed to quantify the amount of cisplatin encapsulated by the calcium phosphate nanoparticles through incorporation during the synthesis in an aqueous medium and adsorption after synthesis, as well as the cytotoxic activity of these formulations in an *in vitro* melanoma model and calculation of the selectivity index in HEK293 cell line.

2.1. Specific objectives

2.1.2. Chapter I

- Quantify the % loading of cisplatin in 91OCis and ne N-Cis by TXRF.
- Calculate the IC50 of the 91OCis, N-Cis, and Cisplatin formulations against the A-375, B16F10 and Hek-293 cell lines.

2.1.3. Chapter II

- Quantify the % loading and the release rate of doxorrubicin of N-Dox.
- Calculate the IC50 of the N-Dox, NPC+Dox, and doxorubicin the A-375 and Hek-293 cells.
- Investigate what is the treatment-induced cell death mechanism.
- Predicting N-Dox cardiotoxicity compared to Dox in H9C2 cells.

CHAPTER I

QUANTIFICATION OF CISPLATIN ENCAPSULATION IN CALCIUM PHOSPHATE NANOPARTICLES AND EVALUATION OF CYTOTOXICITY

Quantification of cisplatin encapsulation in calcium phosphate nanoparticles and evaluation of cytotoxicity

ABSTRACT: Cisplatin is used to treat cancer, but severe side effects limit its clinical use. Several studies demonstrate that the use of nanoparticles as a platform for drug delivery is shown to be a viable alternative to replace traditional chemotherapy, since it uses much lower doses, providing greater bioavailability and reduction in side effects. This study intends to adsorb cisplatin on calcium phosphate nanoparticles (NPC), as well as quantify the encapsulated cisplatin in the 91OCis formulation and evaluate its efficiency as carriers for the delivery of drugs to melanoma cells (A375 and B16F10), and predict the selectivity of the formulations using HEK-293 cells. Total X-ray fluorescence spectroscopy (TXRF) analyzes showed that 91OCis encapsulates 9.6 µg of cisplatin every 1 mg and that NPC cannot adsorb cisplatin on its surface. The formulations were not able to reduce cell viability in the tested cell lines, probably because cisplatin is not released from the nanoparticle structure in the case of 91OCis.

Keywords: adsorption; chemotherapy; nanotherapeutics; TXRF

3. Introduction

Platinum (Pt) derivatives such as *cis*-diamminedichloroplatinum (II) (cisplatin) and carboplatin have been long used in the treatment of cancer, but the side effects are extreme, imposing barriers to the use of these drugs (PINAR et al., 2021). The combination of cisplatin at a concentration of 100 mg/m^2 with carboplatin at 200 mg/m^2 was able to promote progress in the treatment of patients with the alleviation of side effects (GÜVEN et al., 2001).

Pt has an antimitotic activity ruled by a mechanism based on its binding to DNA, RNA, or protein molecules. The formation of these chemical interactions is directly related to the antimitotic and antitumor activity of this compound (MENKE et al., 2021). Pt is eager to make connections with nitrogen 7 from guanines and adenines. These interactions generate adducts between bases located on the same DNA strand or complementary strands. The formation of these bonds can occur with a spacing of at least 105 bases, which allows the incorporation of approximately 10,000 Pt atoms in a single cell (FICHTINGER-SCHEPMAN et al., 1988). Despite this, only 1% of the Pt that is internalized by the cell reaches the nucleus due to the formation of adducts with RNA and cytoplasmic proteins (FUERTES et al., 2012). The inhibition of DNA synthesis and repair by the formation of adducts with Pt is the mechanism responsible for the cytotoxicity of this compound (SUO; LIPPARD; JOHNSON, 1999). This inhibition occurs due to conformational changes caused by the adduct platinum-DNA (SUO; LIPPARD; JOHNSON, 1999).

In work by Zhang, nanoparticles loaded with cisplatin and etoposide proved to be more efficient for treating lung cancer *in vivo* than free chemotherapeutic drugs (ZHANG et al., 2021). Nanotherapeutics is a method that can improve the treatment of cancer by specifically targeting cancer cells and reducing systemic toxicity, however, few formulations are clinically approved (PEER et al., 2007).

The use of nanoparticles with an amorphous structure, such as those composed of phosphates or silicates, for example, are advantageous as agents of drug delivery or imaging. These can retain substances such as proteins, cations, and drugs, present solubility in organic fluids (giving it biodegradability), are tolerated by the mononuclear phagocytic system (extending the pharmacological half-life), in addition to allowing its association with markers (fluorescent, radioactive), magnetic or dense that allow

advantages in obtaining a diagnosis, treatment and monitoring the progression of the disease in a non-invasive way (TABAKOVIĆ; KESTER; ADAIR, 2012).

In this chapter, we evaluated the capacity of calcium phosphate nanoparticles (NPC) synthesized and characterized previously by Alvarenga et al., 2015, of loading cisplatin by adding the drug to the synthesis medium and through post-synthesis adsorption. The quantification of platinum in the formulations was performed by total X-ray fluorescence spectroscopy (TXRF) and the cytotoxic activity of the formulations was evaluated in melanoma cells (A375 and B16F10) and embryonic kidney (HEK293).

4. Material and methods

4.1. Synthesis of 91OCis

The NPC was synthesized using solutions containing phosphate salts at controlled Ph and using a semipermeable membrane system (25 mm wide membrane, MWCO 15,000 Spectrum Medical Industries, Inc.). The experimental conditions and methodology for preparing the NPC are in the form of patent deposits registered under the numbers: BR102012032493-8 and BR102013032731-0. Then, the NPC was separated by centrifugation at 3500 r.p.m. for 10 minutes, discarding the supernatant. The resulting precipitate was washed three times with absolute ethanol and after subsequent centrifugations, dried in a drying oven at 60 °C for 48 hours. Aliquots of 1 mg were placed in conical polypropylene microtubes and sterilized by gamma irradiation, at a dose of 25kGy. The synthesis of 91OCis is carried out in the same way as NPC with the addition of cisplatin to the synthesis medium, allowing the molecules to be trapped in the nanoparticle structure (ALVARENGA et al., 2015).

4.2. Cisplatin adsorption on NPC

A suspension containing 1 mg of NPC was prepared with 300 µL of a stock of 1 mg/mL of cisplatin homogenized using a vortex for 5 minutes. The supernatant was discarded and the pellet was washed with 1 ml of Milli-Q water followed by centrifugation (10 minutes at 20,000x g) 3 times. Functionalization was carried out by addition to the purified pellet 100 µl of a 3% (v/v) hyaluronic acid (HA) and, after further homogenization, 100 µL of 3% (v/v) polyethylene glycol (PEG 400) at room temperature, followed by another homogenization as described previously (TÓTARO, 2017).

4.3. Platinum quantification by TXRF

The three supernatants resulting from the washes (S1, S2, and S3) were reserved for platinum quantification. The pellet formed at the end of the process underwent acid digestion to assess whether there was adsorption of cisplatin. The quantification of the platinum concentration present in the formulations was determined using Total reflection X-ray fluorescence (TXRF) spectroscopy in PICOFOX benchtop spectrometer (Bruker Nano GmbH) as described by Pandey (PANDEY et al., 2021). The concentration of cisplatin (Ccis) was accessed by the equation Eq. (1):

$$Ccis = 100Cpt/64{,}78 \qquad \text{(Eq. 1)}$$

In which the constant 64.78 represents the percentage of the molecular mass of cisplatin composed of platinum and Cpt is the concentration of platinum observed in the analyses.

4.4. Cell culture

The human melanoma cell line (*Homo sapiens*) A-375 was kindly donated by Dr. Helen Lima del Puerto ICB / UFMG, the human embryonic kidney cell line (*Homo sapiens*) HEK-293 was kindly donated by Dr. Marcel Leist, University of Konstanz / Germany, and murine melanoma cell line (*Mus musculus*) B16F10 was kindly donated by Dr. Miriam Paz ICB / UFMG. All cell lines were cultivated in DMEM medium (Sigma Aldrich, USA), containing 10% fetal bovine serum (GIBCO BRL, Grand Island, NY) and 1% antibiotic solution (100 $IU.mL^{-1}$ of penicillin and 100 µg. mL^{-1} of streptomycin (GIBCO BRL, Grand Island, NY)) and kept in a humidified atmosphere with 5% CO2 at 37 ° C.

4.5. Cell Viability Assay

Cell viability was measured using the resazurin assay, according to O'Brien (O'BRIEN et al., 2000). After 48 hours of treatment, 20 µL of 5 µg / mL resazurin was added to each well. The plates were incubated in an oven with 5% CO 2 at 37 ° C for 3 hours. Fluorimetric reading was performed at excitation wavelengths of 530 nm and emission of 590 nm in a plate reader (VarioScan Lux, ThermoScientific®). The number of viable cells correlates with the percentage of reduction in resazurin and will be expressed as a percentage of viability/proliferation according to Eq. (2):

$$\% \text{ viability} = (\text{treatment fluorescence} \times 100) / (\text{cell control fluorescence}) \quad \text{(Eq. 2)}$$

The data are presented in % viability to the control and expressed as mean ± standard deviation from the mean.

5. Results and discussion

TXRF analysis showed that the formulation 91OCis is capable of encapsulating 0.63 ± 0.22 mg / L of platinum (figure 1.), which is equivalent to 0.96 ± 0.33 mg / L of cisplatin. Each 1 mg aliquot of 91OCis contains approximately 31.8 µM of encapsulated cisplatin.

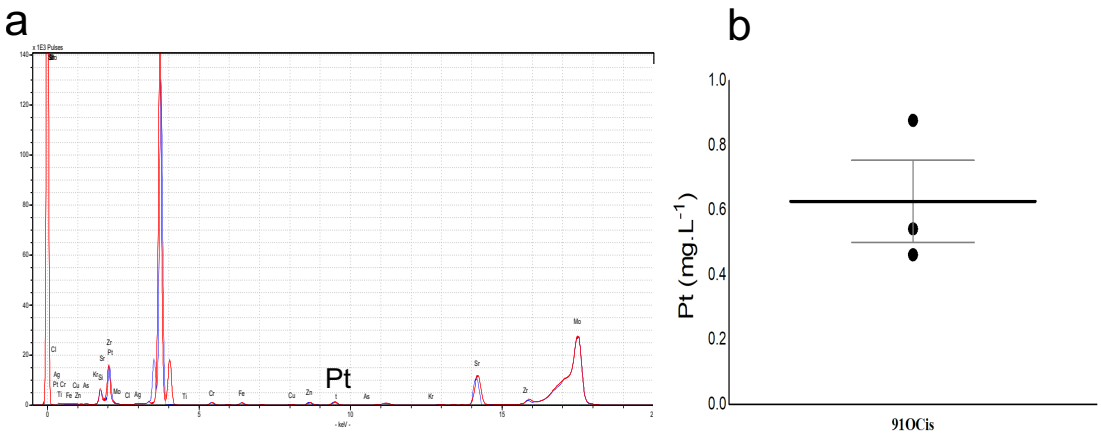

Figure 1. Platinum concentration encapsulated in 91OCis. Representative TXRF spectrogram (a); mean of the platinum concentration measured in samples of three independent syntheses (b). Data expressed as mean ± S.D.

We proceed with the attempt to adsorb Cis to the NPC, which will be called N-Cis. After the interaction between the drug and the nanoparticles, three cycles of washing and centrifugation were carried out, which results in three supernatants (S1, S2, and S3) and a pellet (P) that hypothetically would be loaded with cisplatin. TXRF analysis revealed decreasing concentrations of platinum in supernatants from S1 to S2 (figures 2.a, 2.b) and absence of platinum in S3 (figure 2.c) and P (figure 2.d). In figure 2.e represents the averages of the concentrations found in each stage of preparation.

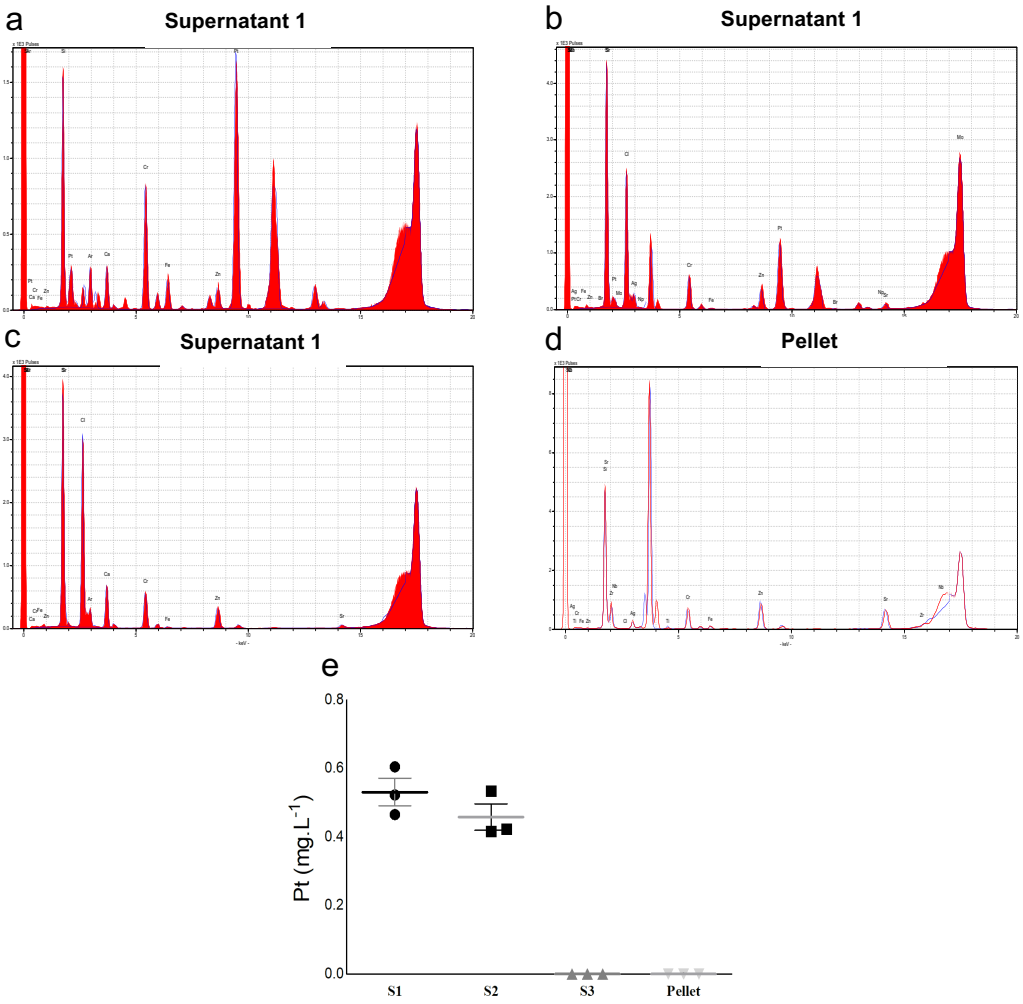

Figure 2. TXRF spectrogram representative of: S1 (a); S2 (b); S3 (c); P (d); means and standard deviation of 3 independent preparations (e).

After the quantification of cisplatin encapsulated in 91OCis and N-Cis, the cytotoxic activity of the formulations was evaluated in the cell lines A375 (figure 3.), B16F10 (figure 4.), and HEK293 (figure 5).

The treatment with Cis was the only one that induced loss of cell viability sufficient to calculate the cytotoxic concentration for 50% of the population (IC_{50}). In cells A-375 (figure 3. a) the IC50 of 48 hours is 0.26 µM ± 0.05, for the cell line B16F10 (figure 4. a) the IC50 for 48 hours is 4.64 µM ± 1.94, while the 48 hour IC_{50} for HEK293 cells (figure 5. a) Is 0.4 µM ± 0.03.

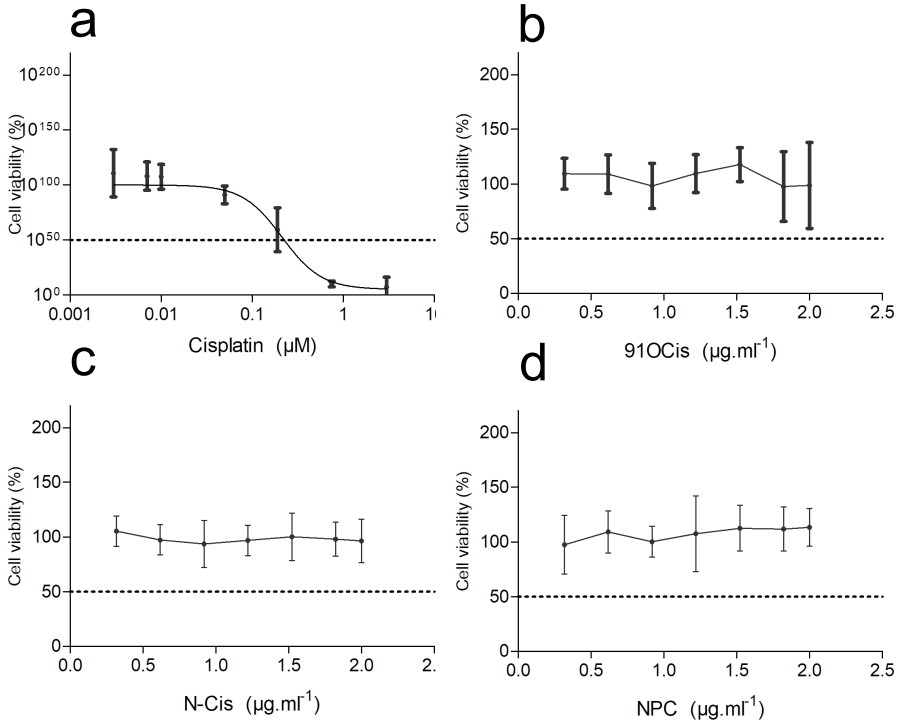

Figure 3. Cis dose-response curves (a); 91OCis (b); N-Cis (c); NPC (d) in A-375 cells treated for 48 hours.

The 91OCis formulation did not reduce the cell viability of A375 cells (figure 3. b.) B16F10 (figure 4. b.) And HEK (figure 5. b.) After 48 hours of treatment as well as N-Cis (A375 - figure 3. c.; B16F10 - figure 4. c. And HEK293 - figure 5. c.) and NPC (A375 - figure 3. d.; B16F10 - figure 4. D. and HEK - figure 5. d.). Thus, it was not possible to calculate the IC50 of these formulations.

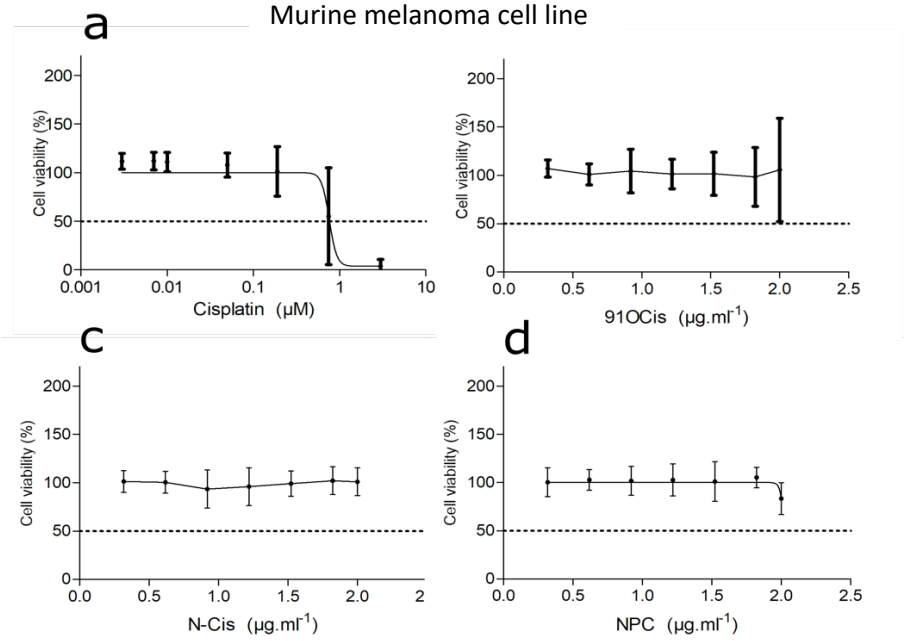

Figure 4. Cis dose-response curves (a); 91OCis (b); N-Cys (c); NPC (d) in B16F10 cells treated for 48 hours.

The absence of cytotoxic activity of N-Cis in conjunction with TXRF analyzes demonstrate that NPC cannot adsorb cisplatin on its surface. In Barroug's work, cisplatin was successfully adsorbed onto crystalline calcium phosphate nanoparticles in Cl^- depleted medium and the adsorption efficiency increases with increasing temperature and decreasing crystallinity (AGGARWAL, 1993).

Although the concentration of Cis in the 91OCis is considerable, it may be strongly linked to the structure of the nanoparticle, which would prevent its release and hydrolysis to activate the cytotoxic mechanism (AGGARWAL, 1993).

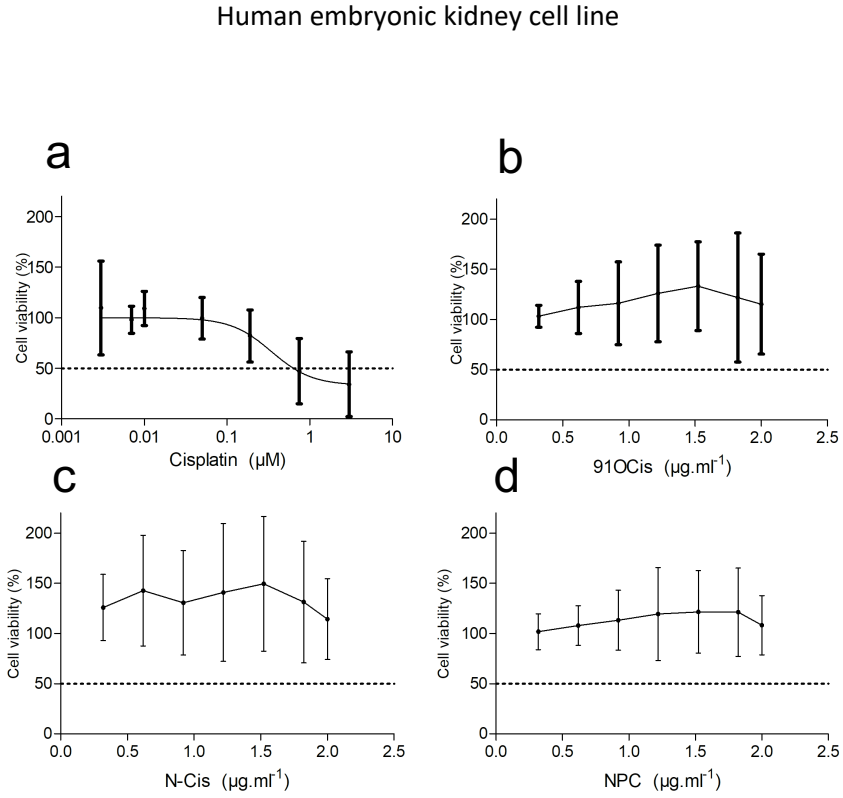

Figure 5. Cis dose-response curves (a); 91OCis (b); N-Cys (c); NPC (d) in HEK293 cells treated for 48 hours.

6. Conclusion

TXRF analyzes demonstrated that the formulation 91OCis is capable of encapsulating 9.6 mg/L of cisplatin, which is equivalent to 31.8 μM in each 1 mg aliquot eluted to the final volume of 1 mL. Also, we demonstrated that NPC cannot adsorb cisplatin on its surface. The cisplatin treatment used as a positive control generated a 48-hour IC50 of 0.26 μM ± 0.05 for A-375 cells, 4.64 μM ± 1.94 for the cell line B16F10, and 0.4 μM ± 0.03 for HEK293 cells. The formulations 91OCis, N-Cis, and NPC do not have cytotoxic activity against the cell lines used in this work.

CHAPTER II

DOXORUBICIN ADSORPTION ON CALCIUM PHOSPHATE NANOPARTICLES IMPROVES ITS ACTIVITY AGAINST MELANOMA CELLS WITHOUT INCREASING TOXICITY FOR CARDIAC PROGENITOR CELLS AND HAS THE POTENTIAL TO BE USED AS AN ADJUVANT

Doxorubicin adsorption on calcium phosphate nanoparticles improves its activity against melanoma cells without increasing toxicity for cardiac progenitor cells and has the potential to be used as an adjuvant

ABSTRACT**:** The incidence rates of melanoma have been increasing dramatically in recent years. The search for strategies that increase therapeutic efficiency and reduce side effects is the focus of several studies today. The treatment mainly uses BRAF kinase blocking drugs, however, several studies have demonstrated the efficiency of doxorubicin hydrochloride to treat melanoma, but the side effects are limiting factors. The association of doxorubicin hydrochloride with nanoparticles is a viable alternative to enhance traditional chemotherapy, aiming at reducing side effects. In this study, doxorubicin hydrochloride was associated with calcium phosphate nanoparticles functionalized with hyaluronic acid and polyethylene glycol and tested in a human melanoma model *in vitro* using the A-375 cell line. The formulations tested showed a significant reduction in IC_{50} over 48 hours when compared to the free drug (Dox 0.44 ± 0.25; N-DOX 0.13 ± 0.07; NPC+DOX 0.16 ± 0.08 μM) and reduced toxicity in HEK-293 cells. The formulation provided a significant reduction in IC_{50} over 48 hours (0.142 ± 0.07) when compared to the free drug (0.44 ± 0.25) and reduced toxicity in HEK-293 cells. Both treatments caused DNA damage, tetraploidy after 72 hours, an increase in the nuclear area, and increased activity of senescence-associated beta-galactosidase. Also, there was no formation of colonies after 14 days of incubation preceded by short exposure treatment. Preliminary results indicate that nano-formulated doxorubicin has potential for melanoma treatment since it potentializes doxorubicin activity without changing the mechanism of action, and does not increase toxicity to H9C2 cells.

Keywords**:** Senescence; antitumor; safety prediction; cardiotoxicity; scapers; adjuvant

1. Introduction

Cancer remains a major issue to public health. In the U.S., it is the second leading cause of death, exceeded only by cardiac failure (SIEGEL et al., 2020). Melanoma is a class of skin cancer that develops quickly and invasively (FATTORE et al., 2017). Its occurrence has been increasing over the years and a prediction made by the American Cancer Society informs that at least 106,110 new cases and 7,110 deaths from melanoma are expected to be reported in 2021 (SIEGEL et al., 2021).

Currently, the first-line treatment suggested for $BRAF^{+}$ melanoma (which are the majority) is based on BRAFq inhibitory drugs that can reduce the proliferative rate (SCHADENDORF et al., 2015). Doxorubicin hydrochloride (Dox) is not currently used as a treatment protocol for melanoma (AZEVEDO et al., 2021). Even so, several studies demonstrated its efficacy in melanoma models (MANSOUR et al., 2003; MOLINARO et al., 2020; ROMANO et al., 2004; YONCHEVA et al., 2019). Despite the benefits, the clinical use of Dox is still a challenge because of a range of serious side effects that includes marked dose-dependent cardiotoxicity and nephrotoxicity (CHATTERJEE et al., 2010; TEYMOURI et al., 2015).

Controlled drug delivery to sites affected by tumors is a desirable strategy to reduces the side effects of chemotherapy (BAE; PARK, 2011). Solid nanoparticles are efficient in delivering drugs to affected tissues (RUENRAROENGSAK; COOK; FLORENCE, 2010). Calcium phosphate nanoparticles (NPC) have the potential to be used in the development of new therapeutic strategies (ALVARENGA et al., 2015). Due to the negative zeta potential (ζ), NPC can adsorb cationic substances (ALVARENGA et al., 2015; PATIL et al., 2007), such as Dox (ZHANG et al., 2016).

The work conducted by Tótaro shows that the zeta potential of NPC became less negative after Dox adsorption. Its elemental composition is predominantly made of magnesium (Mg), calcium (Ca), and phosphorus (P), it has an amorphous nature, spherical shape, and an average diameter of 149 nm (TÓTARO, 2017), which is a desirable size for increased tumor retention (LIU et al., 2013). The adsorption of Dox on NPC was quantified by spectrophotometry, indicating that NPC can adsorb approximately 17.72% of Dox added to the preparation. Furthermore, it was effective against the proliferation of human breast cancer cells (TÓTARO, 2017). However, the possibility of being used as a therapeutic platform for the treatment of melanoma has not yet been investigated.

2. Hypothesis

We hypothesize that using NPC for drug delivery potentiates Dox activity against melanoma cells and does not exacerbate its toxicity to cardiac progenitor cells. To confirm this, the cytotoxicity of a formulation composed of Dox adsorbed on NPC and functionalized with hyaluronic acid (HA) and polyethylene glycol (PEG), was evaluated against the melanoma cell line A375 (*Homo sapiens*). This formulation will be mentioned as N-Dox. The HEK-293 cell line was used as a selectivity model and the H9C2 rat myoblasts were taken as a cardiotoxicity model. Also, part of the mechanism of cytotoxicity induced by treatments was investigated.

3. Material and methods

3.1. Synthesis of phosphate nanocomposites

The NPC was synthesized using solutions containing phosphate salts at controlled Ph and using a semipermeable membrane system (25 mm wide membrane, MWCO 15,000 Spectrum Medical Industries, Inc.). The experimental conditions and methodology for preparing the NPC are in the form of patent deposits registered under the numbers: BR102012032493-8 and BR102013032731-0. Then, the NPC was separated by centrifugation at 3500 r.p.m. for 10 minutes, discarding the supernatant. The resulting precipitate was washed three times with absolute ethanol and after subsequent centrifugations, dried in a drying oven at 60 °C for 48 hours. Aliquots of 1 mg were placed in conical polypropylene microtubes and sterilized by gamma irradiation, at a dose of 25kGy (ALVARENGA et al., 2015).

3.2. Preparation of DOX solution

A stock solution with concentration of Dox at 1.8 mM was prepared. For this, 2 mg of doxorubicin hydrochloride was eluted in 2 mL of deionized water (18 MΩ) cm obtained in a water purification system Mili-Q. After homogenization, 100 µl aliquots were placed in conical polypropylene microtubes and frozen at -20 °C.

3.3. Functionalization of NPC

A stock containing 1 mg of NPC was eluted in 1 mL of deionized water and homogenized with vortex for 5 minutes. A 400 µl aliquot was removed from this colloid, then, the mixture was centrifuged for 10 minutes at 5.000 r.p.m. and the supernatant was discarded. 100 µl of a 3% (v/v) solution of hyaluronic acid (HA) was added to the NPC

pellet and, after re-homogenization, 100 µL of 3% (v/v) polyethylene glycol solution (PEG 400) at room temperature was added to the colloid.

3.4. Functionalization of N-Dox

A stock containing 1 mg of NPC was eluted in 1 mL of Milli-Q water and homogenized using a vortex for 5 minutes. A 400 µl aliquot was removed from this colloid, to which 20 µl of a 1 $mg.mL^{-1}$ (1.8 mM) Dox solution was added and homogenized with the aid of a vortex for 5 minutes. Doxorubicin molecules were adsorbed to the nanoparticle surface. Then, the mixture was centrifuged for 10 minutes at 5.000 r.p.m. and the supernatant was discarded. The centrifugate was resuspended in 400 µl of H_20 milli-Q, centrifuged again for 10 minutes at 5.000 r.p.m., and the supernatant was discarded again. Successive washes ensure that there are no free DOX in the preparation. Was added to the purified pellet 100 µl of a 3% (v/v) HA and, after further homogenization, 100 µL of 3% (v/v) polyethylene glycol (PEG 400) at room temperature, followed by another homogenization(TÓTARO, 2017).

3.5. Preparation of NPC+Dox

To verify the occurrence of influence of the NPC functionalized with HA and PEG in the cytotoxic activity of DOX, a mixture between NPC and Dox was prepared in a 1: 1 ratio. For this purpose, a 100 µl aliquot of the NPC suspension and 100 µl of the DOX stock solution was used, generating a mixture containing 0.6 $mg.mL^{-1}$ of NPC and 0.5 $mg.mL^{-1}$ of Dox (0, 9 mM).

3.6. Dox loading and encapsulation efficiency

The amount of doxorubicin and its loading efficiency in the N-DOX formulation was determined by high-performance liquid chromatography (HPLC) with a UV detector. Aliquots of three independent preparations were analyzed. To determine the loss of mass during the centrifugation process, before proceeding with the functionalization as described previously, the centrifuge microtubes used had their masses checked while empty and again after filling with the properly functionalized N-DOX pellet, purified and oven-dried (37 °C for 24 hours). The difference between the initial mass (IM) of the tube and the final mass (FM) represents the mass of N-DOX mass (MN) recovered after the centrifugation process. To determine the concentration of DOX adhered to the nanoparticles, the functionalized, dry pellet was resuspended in 190 µl of milli-Q water and the volume was made up to 200 µl with a 0.1 M HCl solution. Acidification of the medium promotes the digestion of the material. The solution was analyzed in an ACE C8 column 4.6 mm x 250 mm, 5 µm using a solution of methanol and phosphate buffer 0.01M pH 3.0 in the proportion 65:35 with injection volume 20 µL and flow of 1 $mL.min^{-1}$ and excitation at 470 nm and emission at 555 nm with a fluorescence detector (BORATTO et al., 2020).

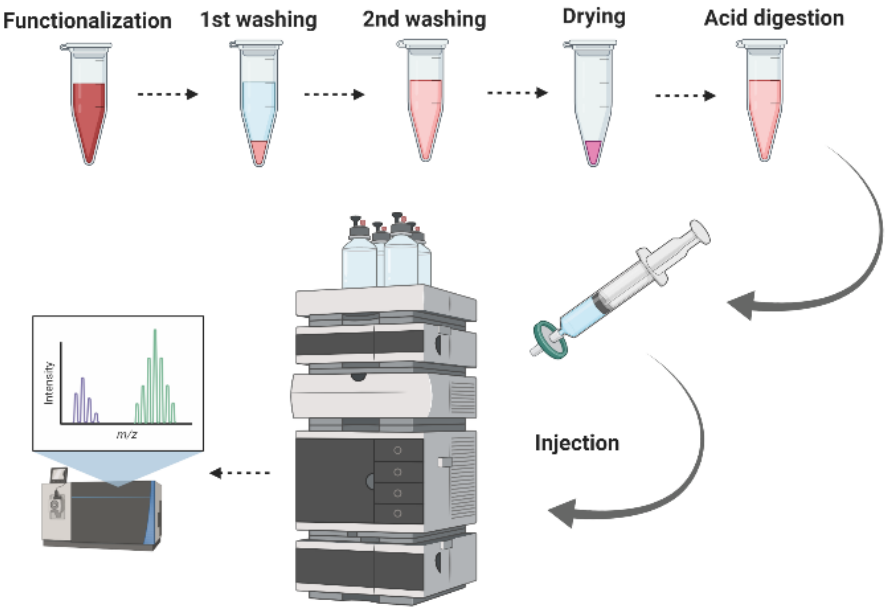

Figure 1. Experimental design of Dox dosage by HPLC.

3.7. In vitro drug release studies

To determine the release rate of doxorubicin from N-DOX, functionalization was carried out in the same way as described above, however, sufficient quantity was prepared so that even with the minimum hypothetical release of 10%, the DOX concentration was within the limit of linearity of the calibration curve. For this purpose, a final volume of 400 µl of N-DOX suspension was prepared with 2.8 mL of NPC [1 $mg.mL^{-1}$] + 140 µL of DOX [1 $mg.mL^{-1}$] (140 µg) in triplicate. This suspension was placed in a bag made with the same type of dialysis membrane used in the synthesis of nanoparticles. The bag was sealed at the ends allowing the dox molecules to pass through the pores of the membrane and the nanoparticles to remain trapped inside. This bag was conditioned in a beaker containing 10 mL of phosphate-buffered saline (PBS) with heating at 37 ° C and constant agitation (figure 1.). The temperature was monitored with the aid of a thermometer and at times of 0.5; 1; 3; 4; 6; 8; 20 h aliquots of 200 µl were removed and

the same volume of medium was immediately replaced to avoid concentration of the samples. The aliquots were analyzed on HPLC as previously described. All analyzes were performed immediately after functionalization.

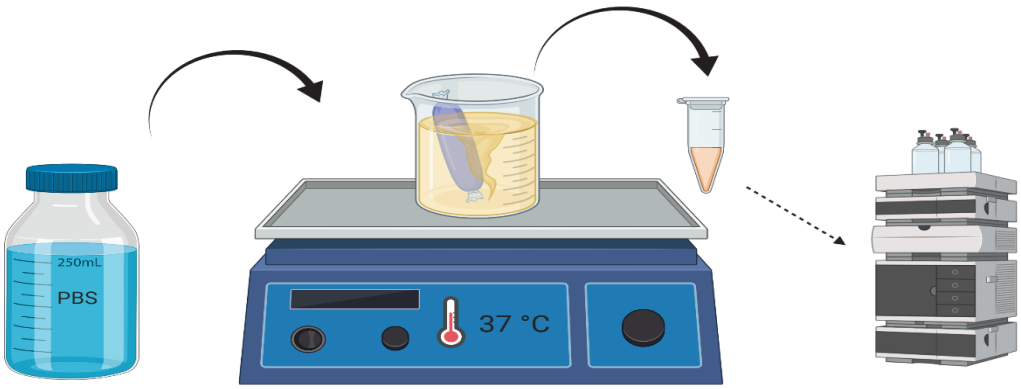

Figure 2. Scheme representing the methodology used for in vitro drug release assay.

3.8. Cell culture

The human melanoma cell line (*Homo sapiens*) A-375 was kindly donated by Dr. Helen Lima del Puerto ICB / UFMG and the human embryonic kidney cell line (*Homo sapiens*) HEK-293 was kindly donated by Dr. Marcel Leist, University of Konstanz/Germany, and rat myoblasts cell line (*Ratus novergicus*) H9C2 was kindly donated by Dr. Luciana Andrade/UFMG. All cell lines were cultivated in DMEM medium (Sigma Aldrich, USA), containing 10% fetal bovine serum (GIBCO BRL, Grand Island, NY) and 1% antibiotic solution (100 $IU.mL^{-1}$ of penicillin and 100 $\mu g.\ mL^{-1}$ of streptomycin (GIBCO BRL, Grand Island, NY)) and kept in a humidified atmosphere with 5% CO_2 at 37 ° C.

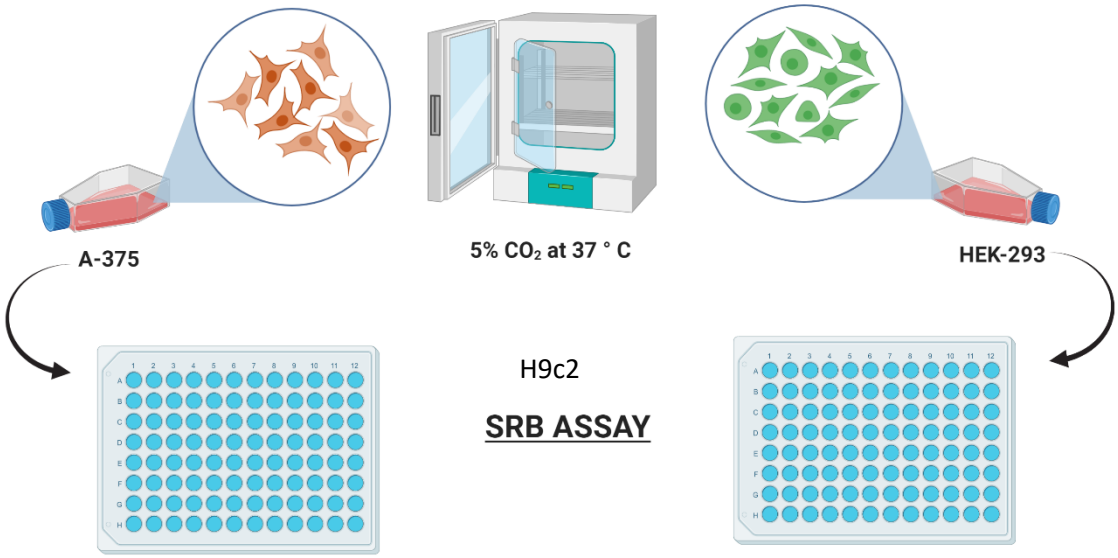

Figure 3. Experimental design of cell culture.

3.9. Cytotoxicity assessment of functionalized formulations

Cell lines A-375 and HEK-293 were seeded at a density of $5x10^3$ cells per well in 96-well plates. The plates were incubated overnight in an incubator with an atmosphere composed of 95% atmospheric air and 5% CO_2, and temperature at 37 ºC for 24 hours until stabilization.

Cell viability was assessed by the colorimetric assay of sulforhodamine B 2-(3-diethylamino-6-diethylazaniumylidene-xanthen-9-yl)-5-sulfo-benzenesulfonate (SRB). For each experiment, two plates were prepared: one for the treatments and the other to be fixed after the end of the stabilization period called "T0 plate" which is used as a reference to assess cell growth, reflecting the quality of the culture. This method directly assesses the occurrence of cell proliferation by quantifying proteins inserted in the plasma membrane of cells in culture. The concentration of proteins can be directly correlated with the rate of proliferation, which is ultimately correlated with cell viability. Quantification is performed by binding the SRB to the membrane proteins of the fixed

cells. This bonding occurs in an acidic medium. After washing, the dye that remained adhered to the cells is solubilized in an alkaline medium, in which the quantification of the optical density (OD) is performed. Thus, the greater the cell biomass present in the well, the greater the concentration of dye adhered to the proteins. Consequently, there will be a higher concentration of SRB in the sample, generating higher values for the reading. Subsequently, the quantification of the optical density can be normalized as the percentage of cell viability observed in each treatment. The method has good sensitivity when compared to the classic fluorimetric methods. Besides, the existence of quality control based on the "T0" plate that is fixed at the time "0" of the treatment, allows to track how much the cells of the control group grew after the start of the treatment time (VICHAI; KIRTIKARA, 2006).

After stabilizing the cultures, the plates were treated with the four formulations prepared (DOX; NPC; N-DOX; NPC+DOX) using eight serial dilutions (1: 5) with concentrations between 180 - 0.05 μM; 120 - 0.007 $\mu g.mL^{-1}$; 1.42 - 0.001 μM; 90 - 0.02 μM + 60 – 0,003 $\mu g.mL^{-1}$ respectively.

To evaluate how the exposure time affects the cytotoxic activity of the formulations, tests with a duration of 24, 48, and 72 hours were carried out. After each treatment period, the plates were fixed with the addition of 90 μL of 10% (v / v) trichloroacetic acid (TCA), incubated for 1 hour at 4 ° C and then washed with tap water four times and oven-dried. After fixation, the plates were stained by adding 50 μL of SRB 0.04% (m / v) to each well for 30 minutes. After staining, the plates were washed four times with 1% acetic acid (v /v) with the aid of a wash bottle. The excess liquid was removed with paper towels and the plates were taken to the drying oven until complete drying. Then, 100 μL of Tris Base pH 10.5 was added to each well and homogenized on the automatic shaker for 5 minutes. After homogenization, the spectrophotometric reading of the absorbance was performed

at 510 nm in a plate reader (Varioskan Lux - Thermo Fisher Scientific ®). The intensity of the optical density is correlated with the number of viable cells (VICHAI; KIRTIKARA, 2006). The experiments were carried out in triplicate in three independent experiments.

Values of cytotoxic concentration for 50% of the population (IC_{50}) were calculated using non-linear regression using GraphPad Prism® software version 5.0 (GraphPad Software Inc). The results were expressed as a percentage of cell viability to the control (PBS 1X) as a function of concentration. The absorbance values (Abs) were normalized as the percentage of cell viability (% VC) considering the absorbance of the PBS-treated control (AbsPBS) as 100% viability, according to the equation (Eq. (1)):

$$\%CV = \frac{(100xAbs)}{AbsPBS} \qquad (1)$$

3.10. Calculation of the selectivity index

The selectivity index (SI) was calculated for each of the formulations: DOX; N-Dox; NPC+Dox as the ratio between the IC_{50} of the HEK-293 cell line and the IC_{50} of the A-375 cells (CHUANG et al., 2015) according to the equation (Eq. (2)):

$$SI = \frac{(\text{IC50 HEK293})}{\text{IC50 } A375} \qquad (2)$$

3.11. Cytotoxicity assessment of non-functionalized formulations

Control cell viability assays were performed to test the efficiency of the functionalization of formulations with HA and PEG as a strategy to improve the targeting of tumor cells and the enhancement of drug activity. Also, the cytotoxic activity of the HA and PEG solution was evaluated.

Immediately after fixing the T0 plate, the plates were treated with the formulations described below: empty and non-functionalized calcium phosphate nanoparticle (NPC^-);

calcium phosphate nanoparticle loaded with doxorubicin and non-functionalized (N-Dox$^-$) and the solution of hyaluronic acid and polyethylene glycol (HA + PEG 1: 1) using eight serial dilutions (1: 5) with concentrations between 120 - 0.0 μg.mL^{-1}; 1.42 - 0.0 μM; 3% - 0.0% (v / v) respectively. The treatment time of 48 hours was chosen for this evaluation due to the higher SI observed when using this protocol. After the treatment period, the plates were fixed and stained as described in topic 2.9. The results were expressed as a percentage of cell viability to the control (PBS 1X) as a function of concentration, calculated as described in the previous topic.

3.12. Quantification of DNA content and evaluation of the cell cycle

The quantification of DNA content and analysis of the cell cycle was performed as described by (RICCARDI; NICOLETTI, 2006). A-375 cells were plated at a density of 5x10^4 cells per well in 24-well plates and incubated overnight. Subsequently, they were treated with DOX, N-DOX, NPC+DOX, and NPC in concentrations referring to the IC_{50} of the treatment of 48 hours 0.45; 0.13; 0.17; μM and 0.6 mg.mL^{-1} respectively. To follow the sequence of events that occur after continuous exposure, the experiments were carried out after 24, 48, and 72 hours of treatment with the aforementioned formulations. After treatment, cells were removed from the bottom of the well with the addition of 50 μL of trypsin-EDTA solution that was inactivated with the supernatant that had been aspirated from the well, homogenized, collected, and centrifuged at 2.000 r.p.m. for 10 min at 4 °C in a micro-centrifuge (Denver Instrument Company, USA). The supernatant was discarded and the cells were labeled with 300 μL of a Hypotonic Fluorochromic Solution (HFS). After 1 h of incubation at 8 °C, the samples were analyzed by flow cytometry (FACSCan®, BD Biosciences). The parameters were acquired and analyzed in the software FlowJo X.0.7® (Tree Star, Inc).

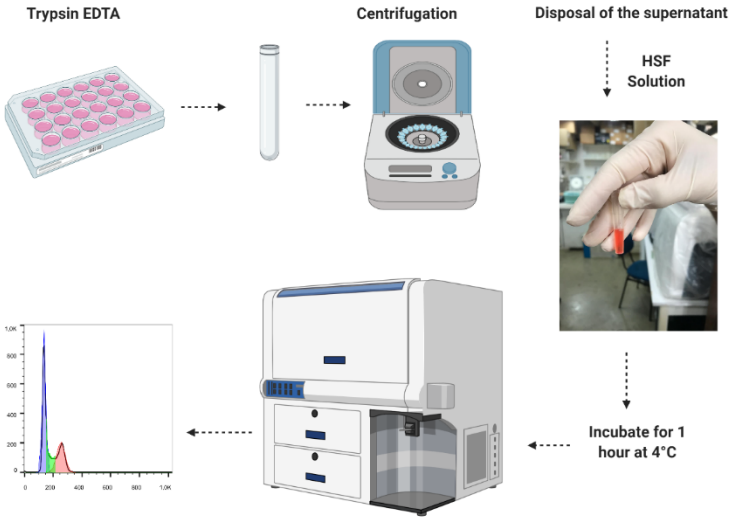

Figure 4. Experimental design of cell cycle analysis.

3.13. Clonogenic assay

The long-term survival of A-375 cells after treatment with the tested formulations was accessed through the clonogenic assay. Long-term trials are essential to correlate the results observed *in vitro* with *in vivo* responses. The clonogenic assay assesses the ability of a single cell to form a colony with at least 50 clones. After the cells suffer treatment-induced damage and the stimulus is removed, the cells may or may not form colonies. Colony formation can be used as a parameter to assess the ability of cells to perform infinite cell divisions (FRANKEN et al., 2006).

The cells were seeded in 6-well plates at a density of 200 cells per well. After 4 hours of incubation at 5% CO2, 95% atmospheric air at 37ºC, the cells received the treatments in the same concentrations used in the cell cycle evaluation assay, and after 24 hours of exposure, the cells were washed and new media added. The plates were incubated for 14 days and then fixed with 4% p-formaldehyde, washed, and stained with 0.1% violet

crystal. Colonies with at least 50 cells were considered and the colonies formed were counted manually. The results are expressed as a fraction of survival, which was obtained by the equations below. Plating efficiency (PE) was determined as the ratio between the number of colonies formed in the well without the treatment and the number of cells seeded, multiplied by 100 (Eq. (3)). The survival fraction (SF) was calculated by dividing the number of colonies that appear after treatment of the cells by the number of seeded cells multiplied by PE (Eq. (4)).

$$PE = \frac{\text{Number of colonies formed by the untreated group}}{\text{Number of seeded cells}} \times 100 \qquad (3)$$

$$SF = \frac{\text{Number of colonies formed by the untreated group}}{\text{Number of seeded cells x PE}} \qquad (4)$$

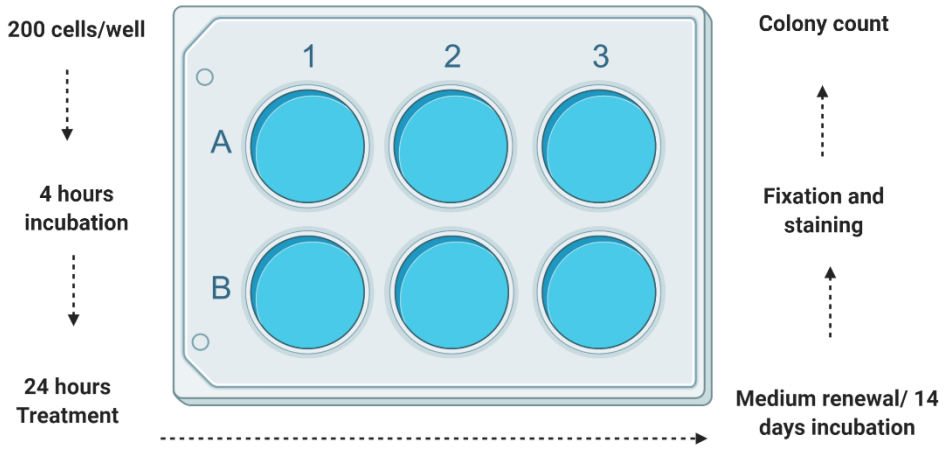

Figure 5. Experimental design of the analysis of the clonogenic assay.

3.14. Quantification of acidic vesicular organelles by FACS

The preliminary assessment of the occurrence of autophagic cell death in A-375 cells was carried out by marking acidic vesicular organelles (AVO) with acridine orange (AO).

A-375 cells were seeded in 24-well plates in the $5x10^4$ density per well and incubated for 24 hours for adherence and expansion. After the culture stabilization period, the wells were treated with DOX, N-DOX, NPC+DOX, and NPC in concentrations referring to the IC_{50} of the time of 48 hours (0.45; 0.13; 0.17; µM and 0.6 $mg.ml^{-1}$), and cell control was treated with PBS. After 24 hours of treatment, the culture medium was aspirated and reserved in identified tubes. Was added 50 µL of trypsin-EDTA to each well and the plates were incubated at 37 ° C for three minutes. After the incubation period, trypsin was inactivated with the culture medium that had been aspirated and returned to its respective well of origin. The cell suspension of each well was homogenized with the aid of a micropipette to break up cell aggregates. Then, the suspension was returned to the tubes mentioned above, and the tubes were centrifuged at 2.500 r.p.m. for 10 minutes. The supernatant was discarded and the precipitate was washed with PBS and centrifuged again. The supernatant was discarded again and the precipitate was resuspended in 300 µL of an AO solution at a concentration of 5 $µg.mL^{-1}$. The reading was performed in a flow cytometer BD™ FACSCan® (THOMÉ et al., 2016).

3.15. Nuclear morphometric analysis (NMA)

A375 cells were seeded at a density of $5x10^4$ cells per well in 8 well Tek Chamber Slides (Nunc™, Thermo Fisher, USA) and incubated for 24 hours for stabilization. Cells were treated as described in topic 2.8. and stained with Hoechst reagent (NucBlue™ Live ReadyProbes™, USA) according to the manufacturer's instructions. The evaluation of nuclear morphometry was carried out by nuclei staining and subsequent measurement of shape and area. These variables were used to calculate the nuclear irregularity index (NII), which is used to indicate the mechanism of cell death induced by treatments. The images were obtained in a confocal microscope (LSM 880 ZEISS, Germany) (magnification x 400) and analyzed using ImageJ software as described by Filippi-Chiella (FILIPPI-CHIELA et al., 2012).

3.16. Intracelular ROS detection

H9C2 cells were seeded at a density of $5x10^3$ per well in 96-well plates and incubated for 24 hours for stabilization before treatment. The cells were treated with 2',7'-

dichlorodihydrofluorescein diacetate (H_2DCFDA) (Sigma Aldrich, USA) at 1 μM in DMEM and incubated for 30 minutes in the dark at 37 ° C and 5% CO_2, then treated with Dox, N-Dox, NPC for 30 minutes. Fluorescence was measured in a multiwell plate reader with excitation at 485 nm and emission at 528 nm (WU; YOTNDA, 2011).

3.17. Senescence associated β-Galactosidase staining

A375 cells were seeded in 24-well plates at a density of $5x10^4$ cells per well, treated as described for cell cycle evaluation, and stained with X-Gal (Thermo Fisher, USA) for cytochemical detection of senescence-associated β-galactosidase (SA-β-Gal) (DEBACQ-CHAINIAUX et al., 2009). Briefly, after the treatment, the cells were washed with PBS, fixed, stained with X-Gal-based solution, and incubated overnight. Images were acquired in a light microscope under 400x magnification. β-gal positive cells were counted manually in Image J software. Data expressed as the relative percentage of positive cells.

3.18. Statistical analysis

All experiments were carried out at least in triplicate. Data were expressed as mean ± S.D. (standard deviation). Statistical analyzes were performed using GraphPad Prism software, version 5.0, GraphPad Software, Inc, USA. The normality of the data was ascertained by the Kruskal-Wallis test and the difference between means of treatments was accessed by One-way ANOVA with Tukey's multiple comparison test. Significant differences were considered at the level of $p \leq 0.05$.

4. Results and discussion

4.1. Characterization of nanoparticles

The zeta potential (ζ) and conductivity, diameter distribution, elemental composition, crystallinity pattern, and NPC's ability to adsorb DOX on its surface were described previously described in the study conducted by Tótaro in 2017 (TÓTARO, 2017).

The zeta potential and conductivity were obtained using the dynamic light scattering technique in the Zetasizer Nano Series (Malvern). The NPC showed zeta potential of -23.0 mV and conductivity of 0.0082 $mS.cm^{-1}$ at neutral pH while N-Dox presented values of zeta potential and conductivity of -14.2 mV and 0.178 $mS.cm^{-1}$ respectively. The diameter distribution was measured by scanning electron microscopy (SEM) and the technique demonstrated that the calcium phosphate nanoparticles have a spherical shape and an average diameter of 149 nm. The elemental composition was determined by x-ray microanalysis, and the presence of magnesium (Mg), calcium (Ca), and phosphorus (P) were found in the composition of the inorganic matrix of the nanoparticles. The structural patterns were obtained by X-ray diffraction and the results indicated that the nanoparticles have an amorphous nature. The adsorption of DOX on the NPC surface was demonstrated by the evaluation of the optical behavior of the washed nanoparticles and the supernatant resulting from the purification process. Spectrophotometric analyzes indicated that NPC can adsorb approximately 17.72% of the DOX mass added to the preparation of the formulation (TÓTARO, 2017).

To confirm the efficiency of loading by dox adsorption in the NPC observed previously, the acid digestion of the purified N-DOX was carried out and the quantification of DOX in HPLC was performed. Table 1. shows the mass of nanoparticles present in each sample, after the washing and centrifugation process, carried out to purify the sample and ensure that the presence of the free drug is negligible according to the methods described by Langer in 2003 (LANGER et al., 2003).

Table 1. Mass of calcium phosphate nanoparticles functionalized with doxorubicin (N-DOX) after purification by washing and centrifugation. Data expressed as mean ± S.D., n = 3.

Sample	Initial mass (mg)	Final mass (mg)
1	0,8	0,6
2	0,8	0,7
3	0,8	0,5
Mean ± S.D.		0,6±0,1

In each batch of functionalization (0.8 mg of NPC and 40 µL of 180 mM doxorubicin hydrochloride and final volume of 800 µL) yield a colloid with an initial concentration of 50 $\mu g.mL^{-1}$ (90 µM). After performing the centrifugation, discarding the supernatant, and subsequent washing in 800 µL of H_2O milli-Q, go through new centrifugation, drying, an amount of doxorubicin remains attached to the nanoparticles. Acid digestion was performed to homogenize the samples to be analyzed by HPLC. The results of chromatographic analysis (figure 6.) showed an average DOX concentration of 14.2 ± 4,8 µM. This result represents an average load (table 2.) of 15.78 ± 5.33%, corroborating the values found by (TÓTARO, 2017) by spectrophotometry. The percentage of the load was calculated based on the equation (Eq. (5)):

$$\%\ \text{of}\ load = \frac{(c.100)}{90} \qquad (5)$$

Where c is the concentration of DOX in the sample in µM and 90 represents the concentration added initially in µM.

Table 2. Dox encapsulation efficiency in NPC and load percentage. Data expressed as mean ± S.D., n = 3.

Concentration µM	% of *Load*
10,4	11,6
19,6	21,8
12,6	14,0
14,2±4,8	15,78±5,33

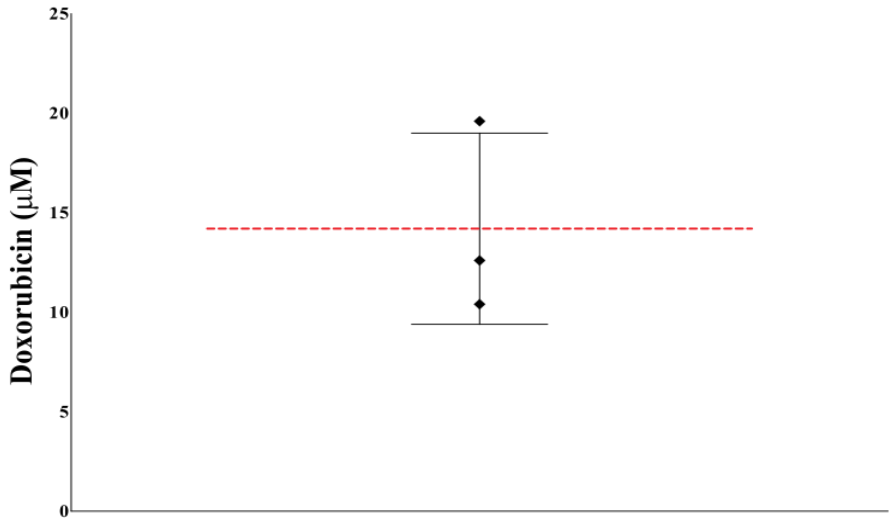

Figure 6. Concentration of Dox adsorbed on NPC. Analysis performed on HPLC after acid digestion, the red dashed line represents the average of the measurements, n = 3, ±S.D.

The NPCs were synthesized in a semipermeable membrane system using solutions containing phosphate salts at controlled pH and loaded with doxorubicin hydrochloride (N-DOX) through electrostatic interactions in a self-assembly reaction in an aqueous medium. This technique makes the process less laborious, less costly, and avoids the use of organic solvents (such as dimethyl sulfoxide) that can increase the toxicity of formulations (SYED; SKONBERG; HANSEN, 2013).

The capacity of a nanoparticle to perform electrostatic interactions with ions and molecules can be modulated according to its ζ (KOSMULSKI, 2009). The occurrence of electrostatic interactions is of paramount importance when a material is designed for biomedical use, especially when this material will be administered intravenously, due to the possibility of interaction with plasma proteins (ZHANG; KOHLER; ZHANG, 2002). Positively charged cerium oxide nanoparticles, with zeta potential ranging from -31.16 to 40.2 mV, showed an increasing ability to adsorb bovine serum albumin (BSA) as the zeta potential increases since BSA is a negatively charged protein. This data was corroborated by an assay in which the pH of the medium was varied. Turning the zeta potential negative, nanoparticles had their ability to adsorb BSA reduced (PATIL et al., 2007).

The loading of DOX in the NPC of the present study follows the same logic. Since NPC has negative zeta potential, it can perform electrostatic interactions with doxorubicin hydrochloride, since it is a cationic compound (ZHANG et al., 2016).

In the study by Zhang et al., 2016 polypeptide nanorods were charged with doxorubicin through electrostatic interactions. The method provided a loading efficiency of approximately 90.2%. This value is considerably higher than that found in this study, however, some methodological peculiarities such as the nanoparticle/drug interaction time and the use of sonication must be taken into account. In this sense, it would be interesting to manipulate the zeta potential to reduce the NPC charge and increase the interaction between the nanoparticle and the drug in the future, to assess whether the loading efficiency is improved.

The coating of the nanoparticles with HA and PEG was carried out by the addition of HA solution (3% v/v) and then mixed with the PEG solution (3% v / v) after resuspension of the washed nanoparticles. Functionalization by adsorption of hyaluronic acid has been previously described and the technique has proved satisfactory for this purpose (BARBAULT-FOUCHER et al., 2002)

The diffusion/release profile of doxorubicin encapsulated in the calcium phosphate nanoparticles is shown in figure 7. Between 1 and 2 hours of incubation at pH 7.4, a burst of release occurs, with a peak in approximately 2 hours (13.9 ± 0.18), where we observe the most notable events. After the early release events, it was observed that there is no increase in the drug concentrations in the medium until the end of the experiment.

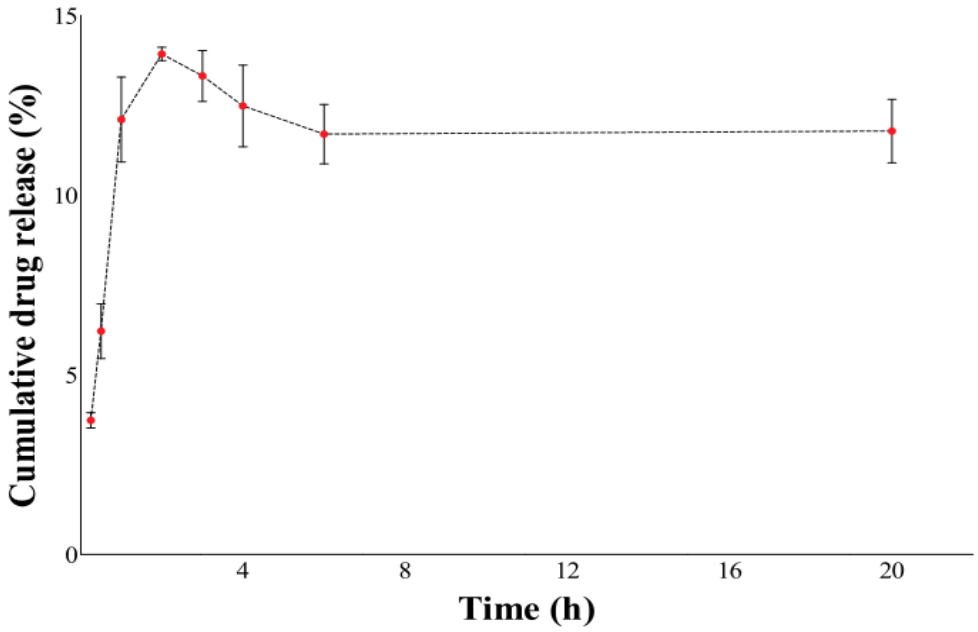

Figure 7. Release/diffusion profile from N-DOX. Initial concentration 25,2 mg.mL^{-1}. Data presented as mean ±S.D., n = 3.

Several factors influence the efficiency of a chemotherapeutic agent, and the plasma retention time is an important factor to be considered. Doxorubicin is administered intravenously and the administration protocol can alter both the pharmacokinetic characteristics, increasing or decreasing the retention time, and as a consequence, modify its antitumor activity (MULLER et al., 1993).

In this context, it becomes imperative that a new formulation increases the plasma retention time of the drug. The data presented in the *in vitro* release test show that a small amount of doxorubicin is released from the surface of the nanoparticle in the first 20 hours. This characteristic is interesting from the point of view that nanocarrier drugs tend to accumulate in tumor tissue due permeability retention (PRE) effect. The anomalous vasculature of the tumor microenvironment has larger intercellular spaces and tortuous paths that cause nanoparticles to accumulate in these sites (IYER et al., 2006).

In addition to the fact that DOX is slowly released from NPCs, previous studies have shown that NPC is capable of transfecting DNA into cells that are difficult to transfect (TONELLI et al., 2015) that is, we are faced with a system with the potential to deliver drugs with specificity (due to the RPE), which enters the nucleus of several cell lines and slowly releases the drug. Thus, it is necessary to conduct a study of biodistribution and clearance *in vivo* to confirm the potential of calcium phosphate nanoparticles containing doxorubicin, to become a tool to increase therapeutic efficacy.

4.2. Assessment of the cytotoxic activity of the formulations

To measure the cell proliferation of the studied cell lines, the SRB colorimetric assay was performed.

To verify the cytotoxicity of DOX in its free and functionalized nanocarrier form, bar graphs were plotted that relate the optical density and the concentration of the tested formulations for the incubation times of 24 hours (figure 8), 48 hours (figure 9), and 72 hours (figure 10) in cell lines A-375 and HEK-293. From the comparison between the quantified optical density for the T0 plate and the treated plates, it was possible to verify cell growth. From this parameter, it is also possible to discriminate if the effect of the formulation is cytostatic or cytocidal.

In A-375 cells treated for 24 hours (figure 8.a), it is possible to observe that DOX has a cytocidal effect, verified by the optical density value, in the highest tested concentration, lower than that detected in the T0 plate. For the nano-carried formulation, N-DOX, we observed that in 24 hours the activity is cytostatic since the absorbance values are close to those observed for the T0 plate even in the highest concentrations (figure 8.b). The formulation composed of the physical mixture of free doxorubicin with the calcium phosphate nanoparticles, NPC+DOX, (figure 8.c), we observed that only at the highest concentration, the optical density found was lower than that measured on the T0 plate. This result indicates that at the 24-hour exposure time, it is necessary to use a higher dose to obtain the cytocidal effect. The empty nanoparticles, NPC, (figure 8.d.), did not show cytocidal or cytostatic activity. This response is evidenced by the absorbance values greater than or equal to the control and therefore, higher than that found on the T0 plate in all concentrations. In the non-tumor cell line HEK-293, for all formulations tested within 24 hours of treatment (Figure 8. e., f., g., and h.), even at the highest concentrations, it was observed that the optical density was always above that quantified in the T0 plate, which suggests cytostatic effect and less toxicity for this line than for the tumor line.

24 hours

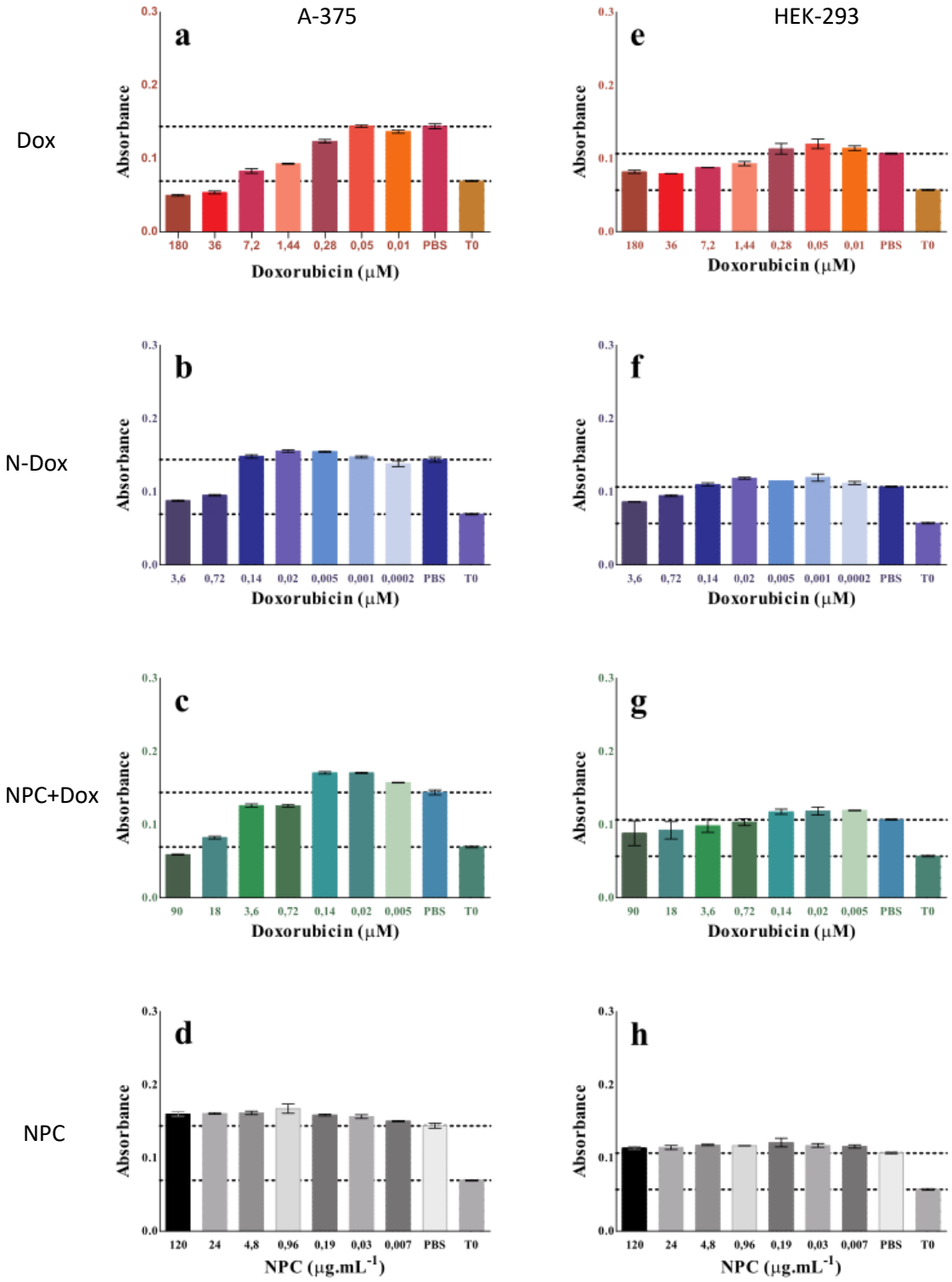

Figure 8. Representative graphs of the optical density of the sulforhododamine colorimetric test performed on A-375 cells exposed to Dox (a); N-Dox (b); NPC+Dox (c)

and NPC (d) and in HEK-293 cells exposed to DOX (e); N-DOX (f); NPC+DOX (g) and NPC (h) for 24 hours of treatment.

The same procedure was performed for 48 hours of treatment (figure 9). For the cell line A-375, the treatment with free doxorubicin, Dox, (figure 9.a) demonstrated a cytocidal effect, verified by the value of optical density, in the highest tested concentrations, lower than that detected in the T0 plate. The same applies to the nano-loaded formulation (figure 9.b) and the formulation composed of the physical mixture of free doxorubicin with the calcium phosphate nanoparticles, NPC+Dox, (figure 9.c). Again, the empty nanoparticles, NPC, showed no cytocidal or cytostatic activity (figure 8.d), a fact evidenced by the absorbance values higher than those found in the T0 plate at all concentrations. In the HEK-293 cell line, Dox (Figure 9. e), N-Dox (figure 9.f), and NPC+Dox (figure 9.g) showed a cytocidal effect only in the highest concentrations. The NPC again showed no activity (figure 9.h) and it was observed that the optical density was always above that quantified on the T0 plate. The cytostatic effect on HEK-293 cells suggests less toxicity for this cell line than for the tumor cell line.

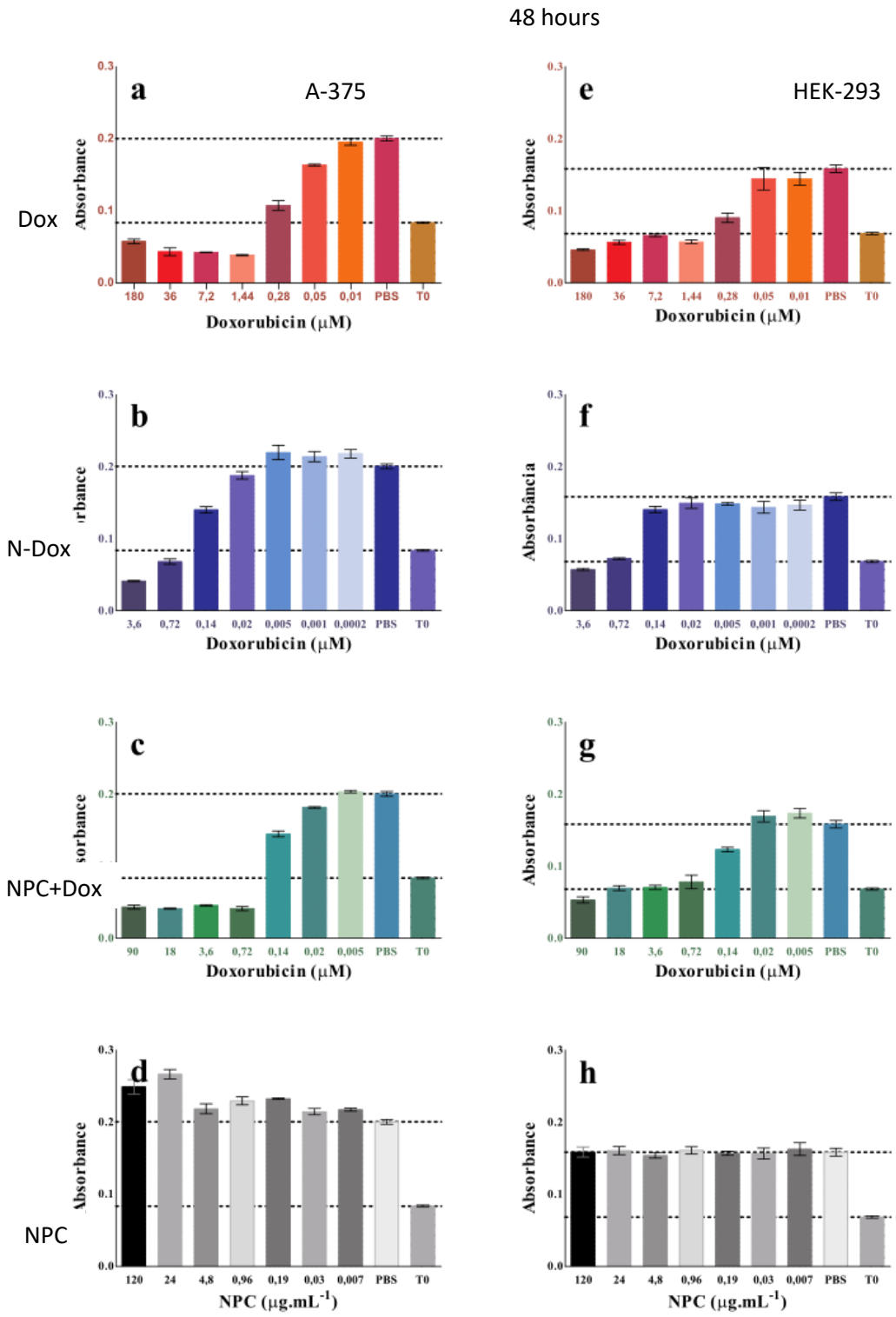

Figure 9. Representative graphs of the optical density of the sulforhododamine colorimetric test performed on A-375 cells exposed to Dox (a); NPC-Dox^{-} (b); NPC+Dox (c) and NPC (d) and in HEK-293 cells exposed to Dox (e); NPC-Dox (f); NPC + Dox (g) and NPC (h) for 48 hours of treatment.

After 72 hours of treatment (figure 10.), the activity profile of the formulations is changed. A general increase in toxicity is observed in all formulations after a long period of exposure. In the A-375 cell line, the three formulations containing drugs: Dox (figure 10.a.), N-Dox (figure 10.b.), NPC+Dox (figure 10.c.) showed potentiation of the cytocidal effect. NPC (without drug) showed reduced cell viability at the highest concentration (120 $\mu g.mL^{-1}$) after 72 hours of exposure for both cell lines (figure 10. d., E., F., G., and h.).

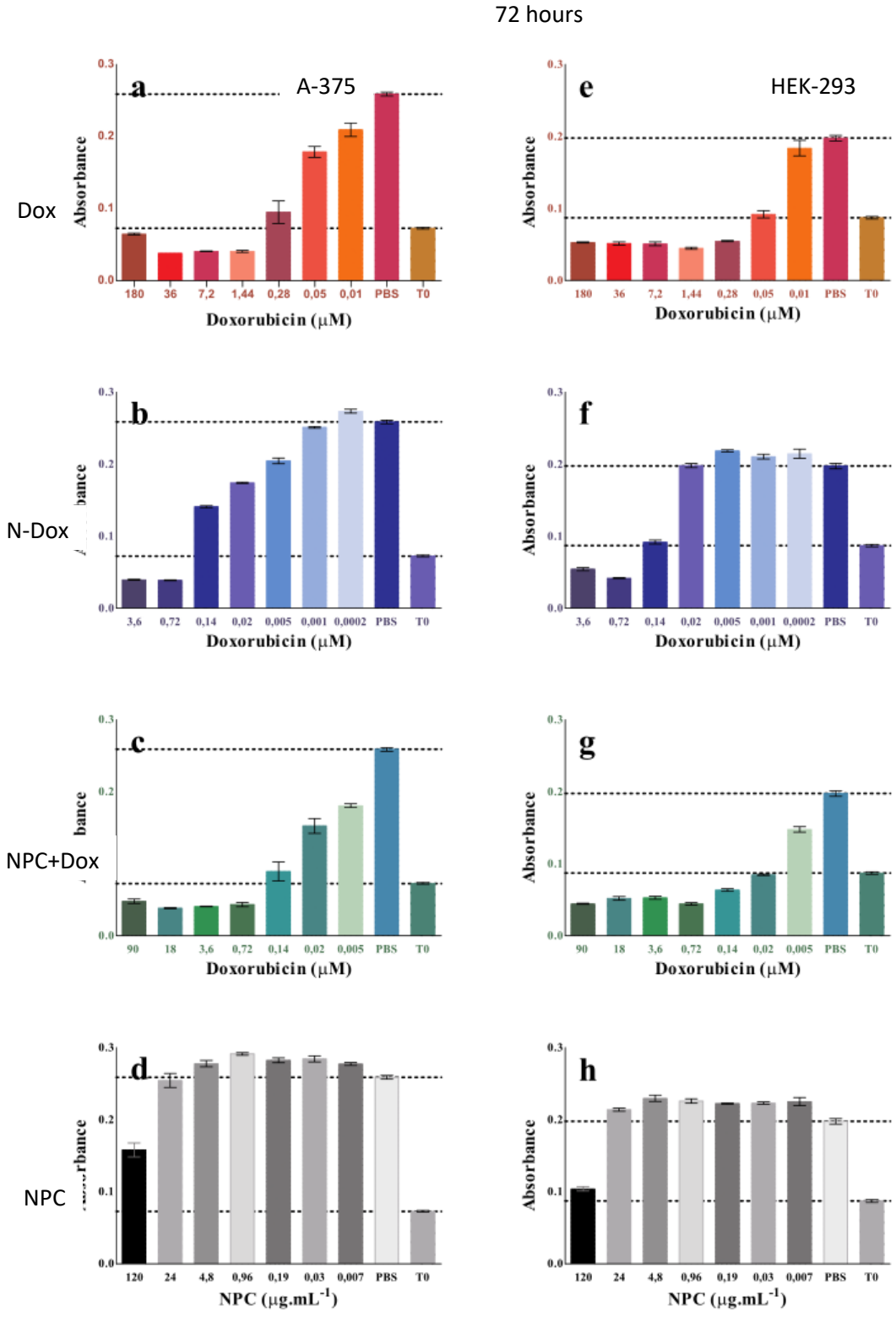

Figure 10. Representative graphs of the optical density of the sulforhodamine colorimetric test performed on A-375 cells exposed to Dox (a); N-Dox (b); NPC+Dox (c) and NPC (d) and in HEK-293 cells exposed to Dox (e); N-Dox (f); NPC+Dox (g) and NPC (h) for 72 hours of treatment.

The values of the concentrations that reduced cell viability by 50% (IC_{50}) of each formulation (table 3.) were calculated from a non-linear regression between the logarithm of the drug concentration contained in the formulations and the percentage of cell viability. PBS treatment was used as a control and was normalized as100% cell viability. IC_{50} values were calculated for 24 hours of treatment, 48 hours of treatment, and 72 hours of treatment (figure 11.) for both cell lines, A-375, and HEK-293. The selectivity index (SI) was calculated as the ratio between the mean IC_{50} of the non-tumor cell line and the mean IC_{50} of the tumor cell line for each formulation tested (figure 12. C). It was not possible to calculate the IC_{50} and SI of NPC since there was no reduction in cell viability after treatment.

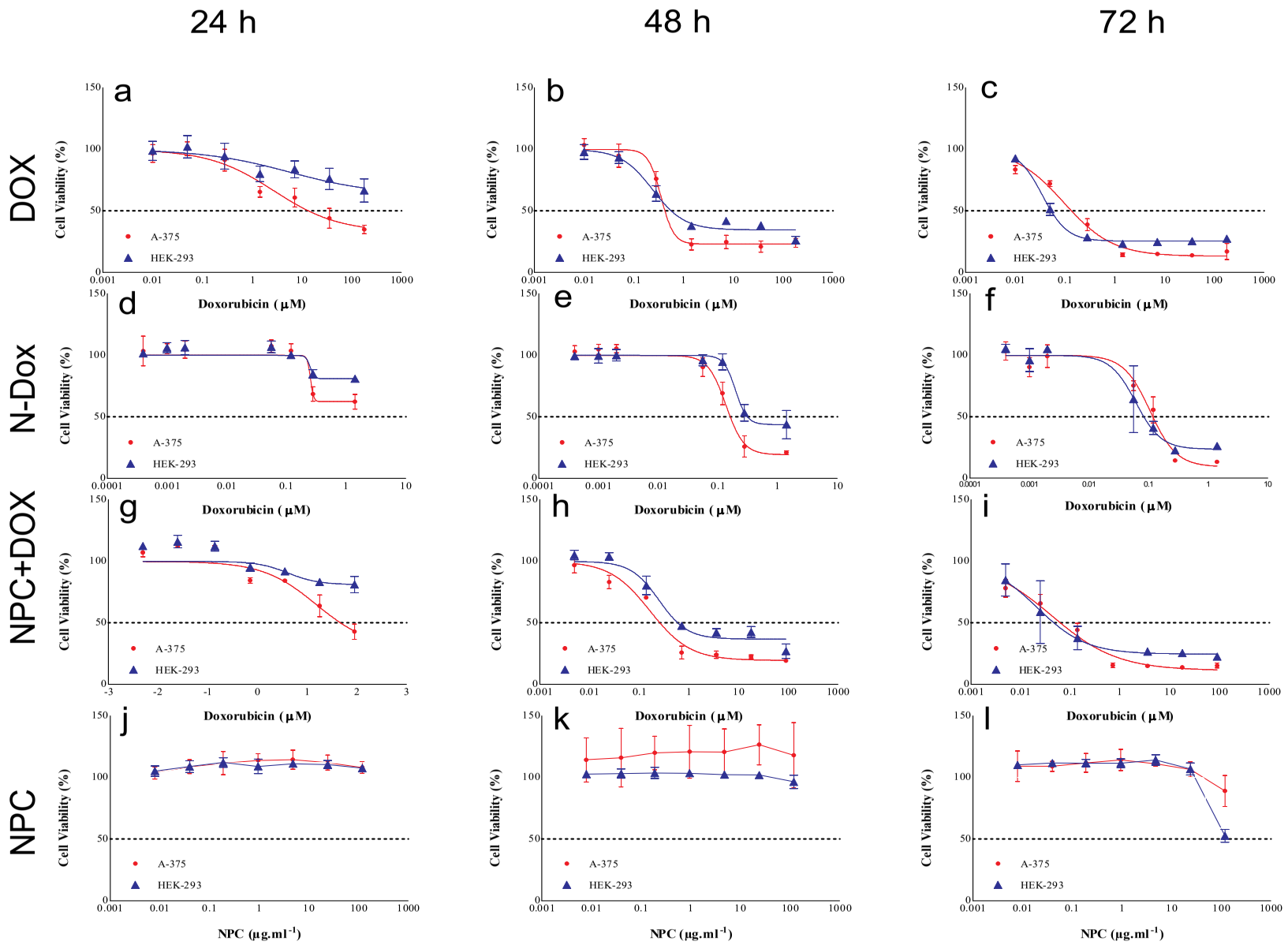

Figure 11. Dose-response curves in cell lines A-375 and HEK-293 after treatment with the formulations: treatment for 24 hours with Dox (a); NPC-Dox + (d); NPC + Dox (g) and NPC (j); treatment for 48 hours with Dox (b); NPC-Dox + (e); NPC + Dox (h) and NPC (k); treatment for 72 hours with Dox (c); NPC-Dox + (f); NPC + Dox (i) and NPC (l).

Since in the first 20 hours only a small amount of drug is released from the nanoparticles, it is expected that the N-DOX formulation will have little cytotoxic activity with the short exposure time treatment. Taking into account that after 20 hours only 13.9% of doxorubicin was released (figure 7.), and since the highest concentrations tested were 3.6 and 0.72 μM, the maximum concentration of the bioavailable drug after that time of treatment would be 0.5 and 0.1 μM (figure 11.d), range in which the IC50 is found (0.23 ± 0.039 μM). These values are much lower than the 24-hour IC50 of doxorubicin for the A-375 cell line found in this study (3.65 ± 2.69 μM) and the values described in the literature: variation of 2.44 μM (MOLLATAGHI, 2019) to 3 μM (ROMANO et al., 2013). A similar effect was observed with polypeptide nanorods loaded with doxorubicin, where the drug's cytotoxic effect against MCF-7 breast cancer cells was enhanced by the association with nanoparticles (ZHANG et al., 2016). There was a significant difference between the IC_{50} of the N-Dox about the DOX during the treatment for 24 hours (figure 12.a.). These results suggest that the activity of the formulations is greater than that of the drug since the interaction of the nanocarrier drug with the cell occurs through different mechanisms.

Doxorubicin is an anthracycline that was initially isolated from the fungus *Streptomyces peucetius.* There are two ways in which doxorubicin exerts its anti-proliferative activity, described in the literature. It can act on both the cytoplasm and the nucleus. After its internalization by the cell, the molecule is reduced to an unstable semiquinone that is transformed again into doxorubicin. This conversion generates reactive oxygen species (ROS) that can generate several cellular damages. The death mechanism induced by ROS is modulated by genes responsible for redox metabolism. On the other hand, the doxorubicin molecule can be directed to the nucleus, where it causes damage to topoisomerase II and alters the expression of genes involved in the process of repairing DNA and cell cycle regulators such as TOP2A, MLH1, MSH2, TP53, e ERCC2 (THORN et al., 2011).

The kinetics of cell viability tests demonstrate that the effect of the formulations varies over time. Correlating these data with the drug release profile, we can suggest that the low cytotoxic activity observed after 24 hours (figure 11. a. d. g. and j) of treatment would be related to the small number of free doxorubicin molecules in the cytoplasm being metabolized and generating ROS. After 48 hours of treatment, the effect of the formulation is enhanced. At this stage, there is an accumulation of damage generated by

oxidative stress and the damage generated by molecules that are being slowly released from the nanoparticles that possibly entered the nucleus and that are causing DNA damage (figure 14.). After 72 hours of treatment, we observed an exacerbated increase in the toxicity of the formulations. Oxidative damage and DNA damage accumulate with the toxicity caused by the nanoparticle (figure 11. l.). Degradation of NPCs due to acidification of the medium may be the reason why prolonged exposure presents marked toxicity. Ca is one of the main elementary components of NPC (ALVARENGA et al., 2015), thus, its degradation can generate an imbalance in the intracellular Ca^{2+} transient, which added to the acute damage caused by doxorubicin, translocate the cell to an irreversible damage state. To confirm this hypothesis, it is essential to mark the signaling of the intracellular Ca^{2+} transients.

The physical mixture, NPC+DOX, (figure 11. g. h. and i.) presented an activity profile similar to that of free doxorubicin. Taking into account that in this system there is the free drug, empty nanoparticles, and nanoparticles with doxorubicin molecules adhered to its surface, we could suggest the occurrence of both of the mechanisms suggested above (THORN et al., 2011). Thus, the formulation presents potentiation of the effect of the drug, however, the reduction in toxicity is not as marked as that observed in N-Dox (figure 11 d. e. and f.).

Table 3. Cytotoxicity, IC50 [μM], and selectivity index of formulations in cell lines A-375 and HEK-293. Values were expressed as the average of 3 independent experiments ± SD and uncalculated values represented by "NC".

	A-375						HEK-293		
	24 h		48 h		72 h		24 h	48 h	72 h
Formulation	IC_{50}	SI	IC_{50}	SI	IC_{50}	SI	IC_{50}	IC_{50}	IC_{50}
DOX	3,65 ± 2,69	<1	0,44 ± 0,25	<1	0,16 ± 0,05	<1	1,05 ± 0,47	0,24 ± 0,12	0,04 ± 0,005
N-DOX	0,23 ± 0,039	<1	0,13 ± 0,07	3,20	0,09 ± 0,04	<1	0,22 ± 0,075	0,43 ± 0,22	0,1 ± 0,07
NPC+DOX	21,4 ± 13,23	<1	0,16 ± 0,08	1,52	0,04 ± 0,02	<1	3,1 ± 1,4	0,25 ± 0,16	0,01 ± 0,001
NPC-DOX^{-}	NC	NC	0,42 ± 0,1	NC	NC	NC	NC	NC	NC
NPC	NC	NC	NC	NC	NC	NC	NC	NC	NC
NPC-HA+PEG	NC	NC	NC	NC	NC	NC	NC	NC	NC

The search for new drugs and more efficient formulations is still a major challenge for scientists. Much of the problems associated with this issue are related to the prediction of toxicity and safety for use. The difficulty of verifying different levels of toxicity in different organs is still a significant barrier. In the last decades, the use of *in vitro* models has proven to be efficient to access the security of new technologies and direct research promoting the policy of the three R's (replacement, reduction, and refinement) for using animals in research (GOH et al., 2015).

To confirm the existence of significant differences between the IC_{50} of the formulations, a ONE-WAY ANOVA was performed with Tukey's average test (figure 12. a). The result of the analysis showed that after 24 hours of treatment, only NPC+DOX^{+} showed a significant difference concerning DOX in the cell line A-375. Within 48 hours, the potentiation observed in the formulations N-Dox and NPC+DOX showed a significant difference to DOX. At 72 hours, only the N-Dox formulation showed a significant difference to DOX. In the HEK-293 cell line, no IC_{50} formulation showed a significant difference regardless of which formulation or time was evaluated.

The selectivity index (SI) is defined as the ratio between the IC_{50} of the non-tumor line and the IC_{50} of the tumor line [$SI = IC_{50HEK\text{-}293}/IC_{50A\text{-}375}$]. As in the observed values of IC_{50}, naturally, the selectivity index shows the same pattern of variation (figura 12. c.). The 48-hour treatment time appears to be the optimized time for treatment with the tested formulations due to the potentiation of the drug's effect with increased selectivity by the tumor line. In figure 9. we observe the variation of the IC_{50} over time in the tumor cell line (figure 8.a.) and non-tumor cell line (figure 12.b.). It is observed that in 24 the activity

of the formulations is low and after 48 hours of treatment, the effect is more strongly enhanced in the cell line A-375 than in the cell line HEK-293, which resulted in an increase in the index of selectivity for this treatment time. After 72 hours, potentiation continues to increase, however, the accentuation of the cytotoxic effect in the HEK-293 cells reduces the SI, suggesting an increase in the systemic toxicity of the formulations (CEZAR, 2007).

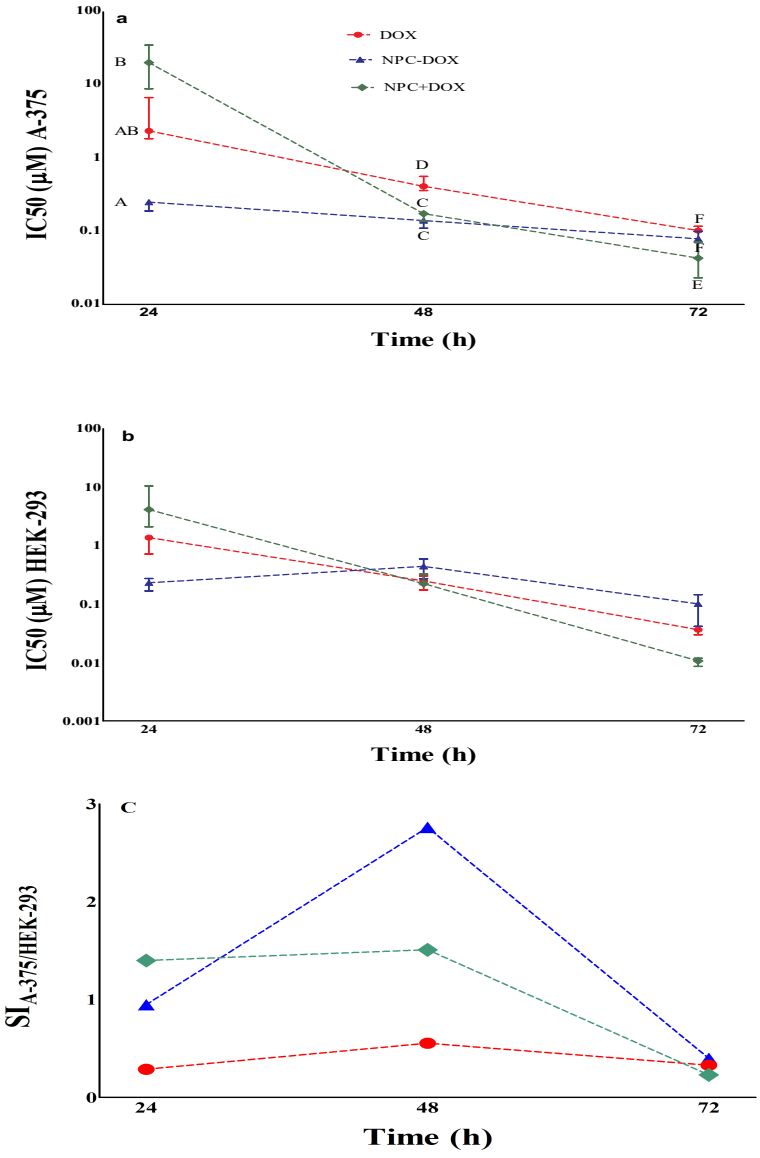

Figure 12. Comparison between IC_{50} after 24, 48, and 72 hours of treatment with DOX, N-DOX, and NPC+DOX in cell lines A-375 (a); comparison between IC_{50} after 24, 48, and 72 hours of treatment with DOX, N-DOX, and NPC+DOX in cell line HEK-293; variation in the selectivity index over time (c). The results were compared by ANOVA and Tukey's mean comparison with a significance level at p <0.05. The letters indicate a significant difference between treatments.

After determining the IC_{50} values and the selectivity index of each formulation, the rate of potentiation of the drug was determined by calculating the ratio between the mean IC_{50} of Doxorubicin and the mean IC_{50} of the formulations in the respective cell lines (Table 4.). The IC_{50} value for all formulations at the respective treatment times (24, 48, and 72 h), were calculated using the software Graphpad Prism® 5.0 (GraphPad Software Inc). Values greater than 1 represent potentiation of the drug's action while values minor than 1 mean reduction in its activity.

Table 4. Increase/decrease of the potency of the formulations to doxorubicin hydrochloride in cells A-375 and HEK-293.

	A-375			**HEK-293**		
	Increased activity					
Formulation	24 h	48 h	72 h	24 h	48 h	72 h
N-DOX x **Dox**	15,9 x	3,4 x	1,8 x	4,8 x	0,6 x	0,4 x
NPC+DOX x **Dox**	0,2 x	2,8 x	4 x	0,3 x	1,0 x	4 x

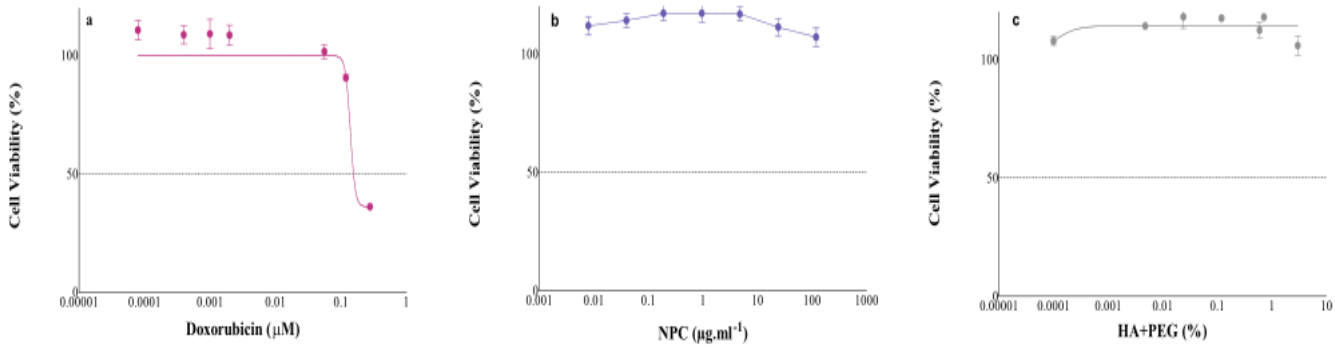

Figure 13. Dose-response curves after 48 hours of treatment with NPC-Dox^{-} (a); NPC^{-} (b); HA + PEG (c) in the A-375 cell line.

To assess the efficiency of targeting to A-375 cells hypothesized by the functionalization of nanoparticles with HA and PEG, the formulations were prepared without functionalization: nanoparticles loaded with DOX without functionalization with HA and PEG (NPC-Dox-) (figure 13. a.), and the empty non-functionalized nanoparticle (NPC^{-}) (figure 13. b.). The cytotoxicity of the HA and PEG solution (1:1) was also investigated for purposes of experimental control (figure 13.c.) The 48-hour treatment time was chosen because it had the highest selectivity index.

The results of these cell viability assays demonstrated that the functionalization of calcium phosphate nanoparticles with hyaluronic acid and polyethylene glycol is an important protocol to increase the efficiency of the formulation. The reduction in cell viability was minor when this step was omitted from the preparation of the formulation. It was also demonstrated with this test that NPC's are non-toxic within 48 hours regardless of functionalization (figure 13.b.). Finally, it is also observed that HA and PEG alone do not have cytotoxic activity (figure 13.c.), despite actively acting in the potentization of the nanocarrier system. This effect was proven through the Student's T-test that compared the IC_{50} of the functionalized formulation with the IC_{50} of the non-functionalized formulation (figure 10.). The IC_{50} of the non-functionalized formulation was significantly higher than the IC_{50} of the functionalized formulation.

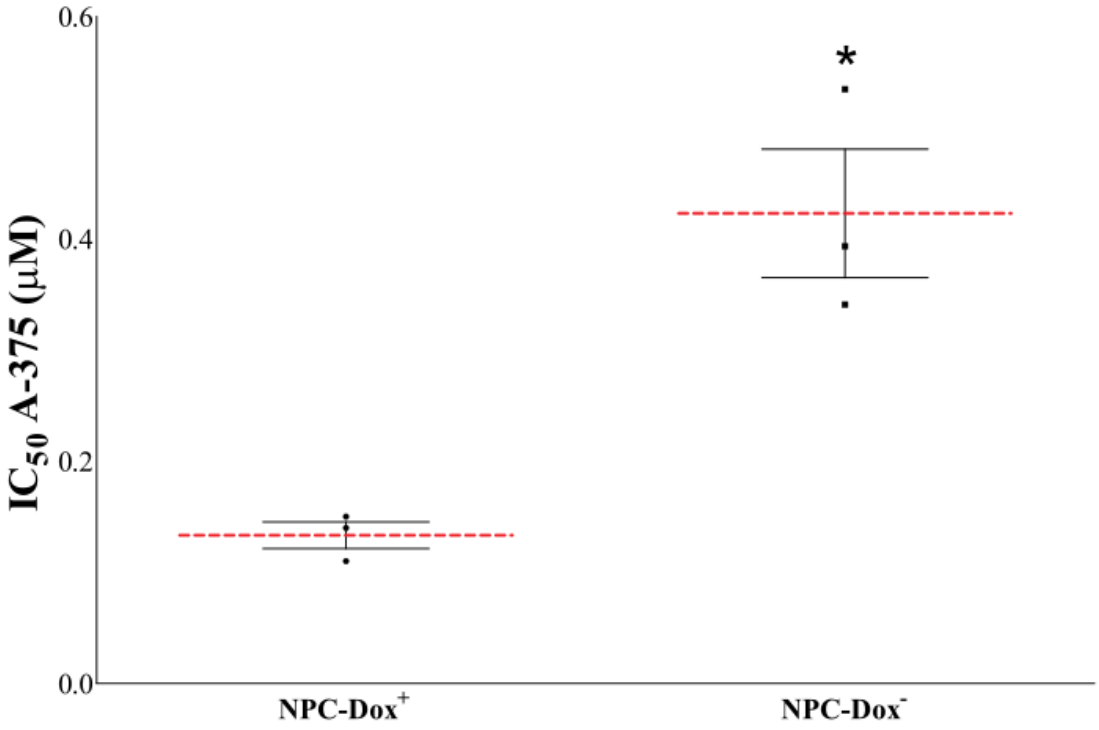

Figure 14. Comparison between the 48 hours IC_{50} of N-Dox (functionalized) and NPC-DOX^- (non-functionalized) in the A-375 cell line showing the potentiation of cytotoxicity with functionalization. The results were compared with the Student's t-test with a significance level of $p < 0.05$. * indicates a significant difference between treatments. The red dashed line represents the average of the measurements.

HA is an abundant component of the extracellular matrix and plays important role in cell proliferation, migration, and survival (KAROUSOU et al., 2017). The regulatory activity of this molecule on cells occurs through its interaction with the CD44 receptor (ARUFFO et al., 1990). The CD44 receptor is overexpressed in several types of tumors,

including melanoma (DIETRICH et al., 1997). Thus, the use of HA as a targeting molecule for drug delivery systems is an advantageous strategy because, in addition to being strongly bound to CD44 receptors, it is biocompatible and biodegradable (ASSARAF et al., 2019). The reduction in cytotoxicity observed in the non-functionalized formulation possibly occurred due to the reduction in the cell uptake of nanoparticles in the absence of the interaction between hyaluronic acid and CD44 receptors. Other studies demonstrate that the coverage of nanoparticles with hyaluronic acid is efficient to increase targeting to areas affected by tumors (ASSARAF et al., 2019).

To determine whether the reduction in viability observed in the cell viability assay was associated with damages in cell cycle progression, the DNA content of A-375 cells after treatment with DOX, N-DOX, NPC+DOX, and NPC in the concentrations referring to the IC_{50} of the time of 48 hours (0.45; 0.13; 2 $\mu g.ml^{-1}$/0.16 µM; and 0.6 $mg.ml^{-1}$ respectively) and cell control was treated with PBS. The IC_{50} referring to the 48-hour treatment time was chosen since it had the highest SI. To record the occurrence, and evaluate the DNA fragmentation kinetics, the experiment was carried out with readings after 24, 48, and 72 hours of exposure. This experimental design allows us to monitor the activity of the compounds in a kinetic way (figure 15.).

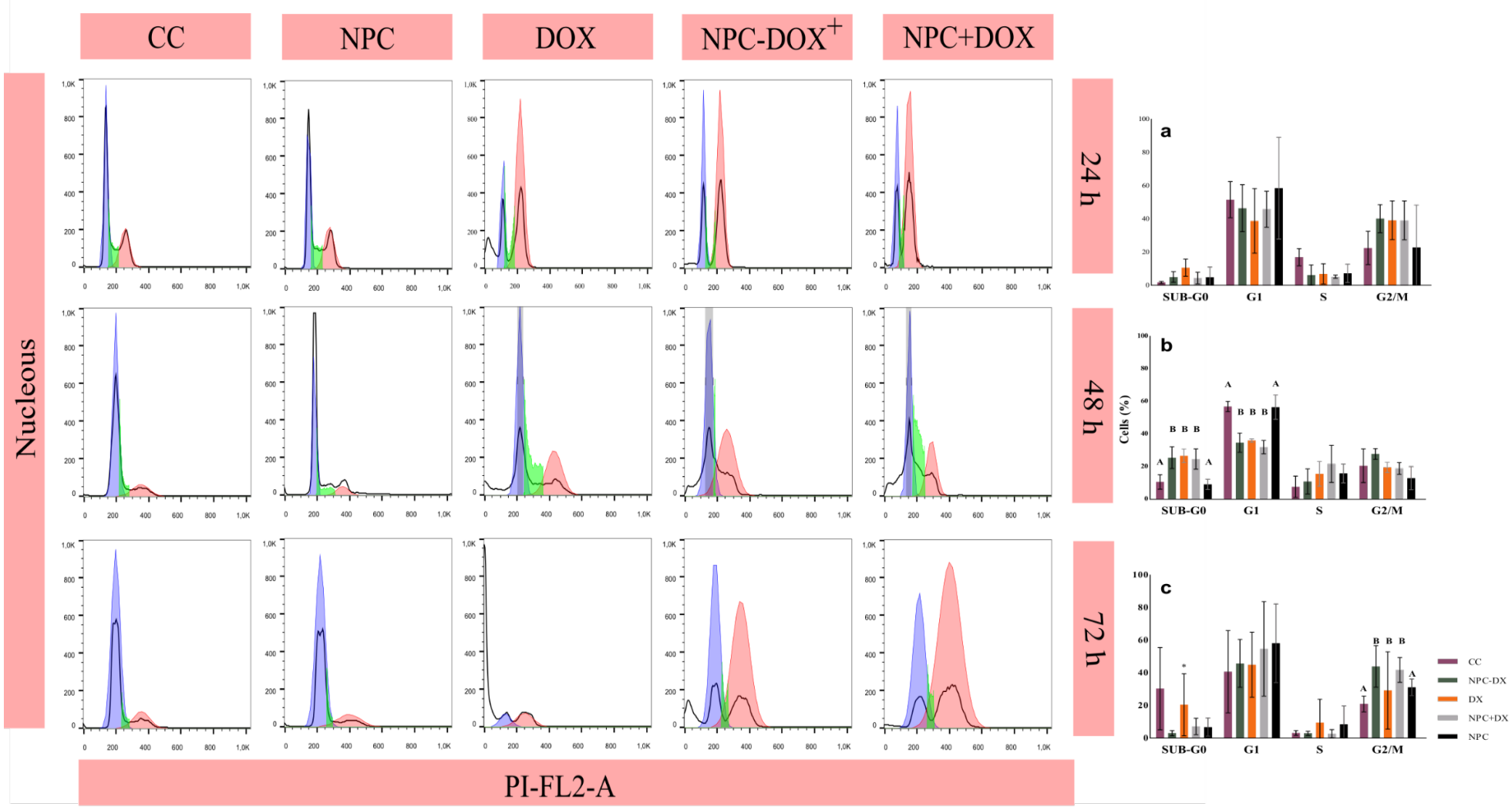

Figure 15. Effect of DOX treatment (0.45 µM); NPC-DOX + (0.13 µM); NPC + DOX (2 µg.ml-1 / 0.16 µM) and NPC (0.6 mg.ml-1) on the cell cycle of A-375 cells. Representative histograms of cell percentage according to the phases of the cell cycle. 24-hour treatment (a); 48-hour treatment (b); 72-hour treatment (c). The data are presented as mean ± SD obtained from three independent experiments carried out in duplicate. The data were compared by ANOVA and Dunnett's means test with a significance level at $p < 0.05$. The letters A and B show a significant difference between treatments.

The treatment with NPC did not cause any change in the cell cycle. Treatment with N-Dox (0,15 μM) and Dox (0,45 μM) in A375 cells did not induce significant changes in cell cycle progression after 24 hours of treatment (figure 15. a.). In the study conducted by Filippi-Chiela and collaborators, glioblastoma cells treated with revosterol for 24 hours showed cell cycle arrest in G2/M and an increase in the number of autophagosomes marked with acridine orange (AO) concomitant with increased expression of Atg5 autophagy regulatory proteins, beclin-1 and LC3-II. When the cells were previously treated with 3 MA, an inhibitor of the enzyme phosphatidylinositol 3-kinase, an enzyme essential for the progression of the autophagic process, there was a significant reduction in the autophagy markers and the inhibition of autophagy reversed the effect observed, indicating a correlation between the cell cycle arrest in G2/M with the occurrence of autophagy. Besides, autophagy and apoptosis occurred simultaneously after treatment. Inhibition of both (autophagy and apoptosis) canceled out the cytotoxic effect of resveratrol (FILIPPI-CHIELA et al., 2011). Thus, cell cycle arrest in G2 / M can be used as an indication of the induction of autophagic cell death in the first hours of treatment.

On the other hand, within 24 hours it is already possible to observe the occurrence of DNA fragmentation in the treatment with DOX. The treatment with NPC did not cause any change in the cell cycle at that time of treatment. After 48 hours of treatment, we observed a significant increase in DNA fragmentation caused by treatment with DOX, N-DOX, and NPC+DOX both concerning cell control as well as treatment with NPC (figure 15.b.) which is a strong indication of the occurrence of programmed cell death (BORTNER; OLDENBURG; CIDLOWSKI, 1995). Also, these treatments led to a significant reduction in the number of diploid cells (G0 / G1) compared to control and treatment with NPC. There was no significant increase in the population of cells in phase S. After 72 hours of treatment (figure 15.c.), it was observed that there is a significant increase in the number of tetraploid cells. Tetraploidy can be chemically induced in mammalian cells through direct interference at the checkpoints of the cell cycle. When cells leave the mitotic phase without the proper occurrence of chromosomal segregation or cytokinesis, the formation of tetraploid cells is possible. Microtubule inhibitors such as colchicine, are capable of inducing the formation of tetraploidy as well as taxol that induces cell cycle arrest in the mitosis phase (ANDREASSEN; MARTINEAU; MARGOLIS, 1996). As no significant difference in cell cycle progression was observed

after treatment with N-Dox concerning Dox, we suggest that the formulation does not alter the mechanism of action of doxorubicin.

Based on the results observed in the cell cycle kinetics test, where was observed cell cycle arrest in S-G2 / M after 72 hours, there is a possibility of occurrence of autophagic cell death caused by 24-hour treatments. To verify this hypothesis, acid vesicular organelles (AVO) were marked with acridine orange (AO) for quantification by flow cytometry. This fluorochrome emits green fluorescence in a neutral environment and starts to emit red fluorescence in an acid environment after it is protonated. When the formation of AVO occurs, the AO is retained inside the organelle and the red fluorescence is captured in the FL-3 channel of the flow cytometer (GOUSSETIS et al., 2010). The analysis carried out by flow cytometry showed the formation of OVA in the A-375 cells treated with DOX, N-DOX, and NPC + DOX in concentrations referring to the IC50 of the 48 hours treatment but there was no OVA formation in the group treated with NPC, as well as in the control group (figure 16.). To find out if there is a significant difference in the number of OVA formed in each treatment, the results were analyzed using ONE-WAY ANOVA with Tukey's mean test.

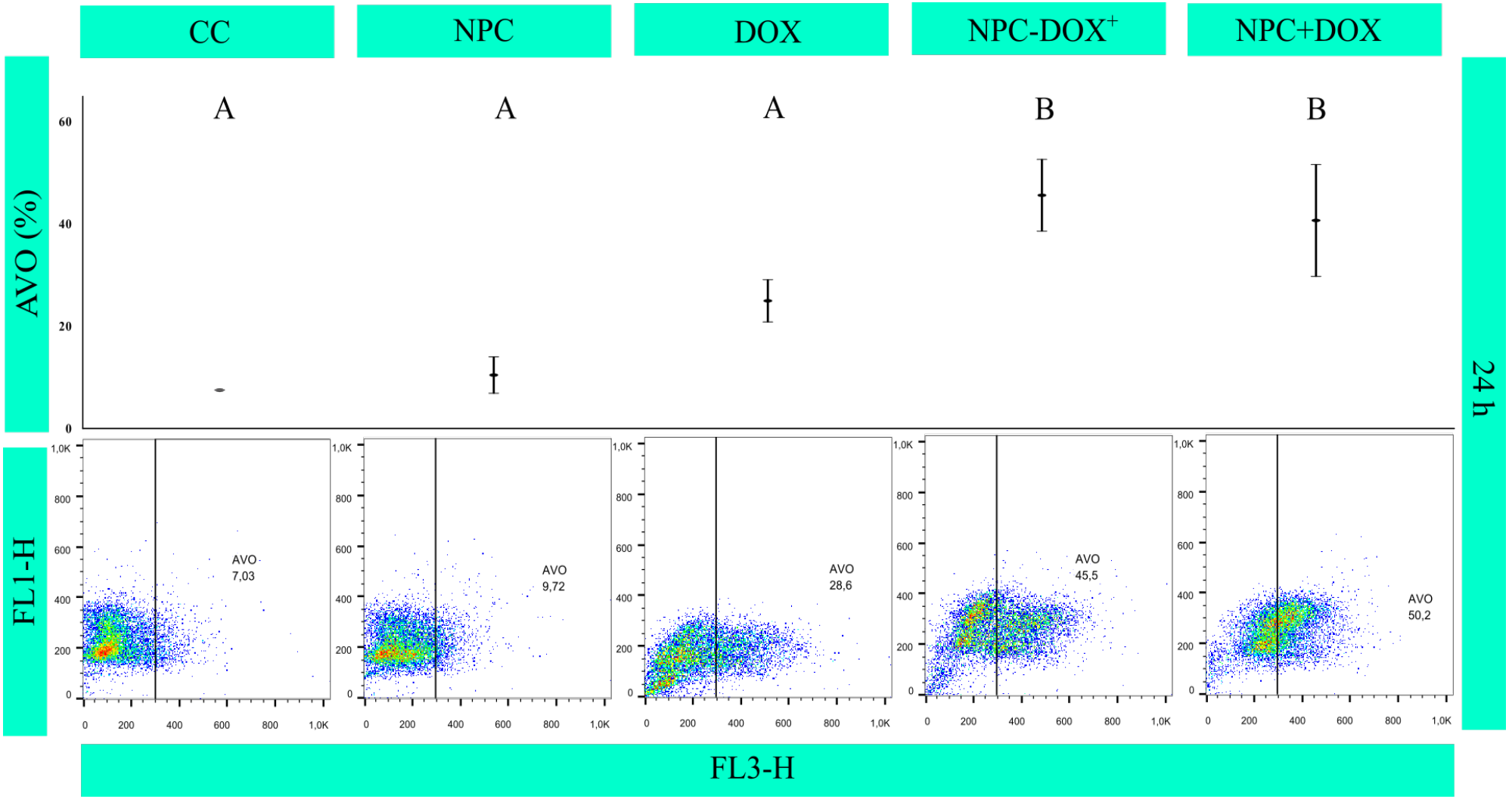

Figure 16. Evaluation of AVO formation in A-375 cells after 24 hours of treatment with CC; NPC; DOX; N-DOX and NPC+DOX. Cells are marked with acridine orange and analyzed by flow cytometry. The data are representative of three independent experiments carried out in duplicate, n = 6. The results were compared by ANOVA with Tukey's mean test at a significance level of $p < 0.05$. The letters A and B indicate a significant difference between treatments.

The formulations N-DOX and NPC+DOX induced the formation of more OVA when compared to the control group as well as to the treatment with NPC (figure 16). The treatment with DOX, on the other hand, induced the formation of OVA, however, the amount formed does not differ significantly from the control. The same occurred with the NPC, there is no significant difference in the number of OVA concerning the control, reinforcing the hypothesis of its non-toxic nature.

To ascertain this hypothesis and get an indication of which cell death mechanism is activated by treatments, we proceeded with the staining of the cell nuclei with Hoechst (figure 18.b.) and subsequent Nuclear Morphometric Analysis (FILIPPI-CHIELA et al., 2012). The data demonstrated that the treatments triggered the occurrence of large and regular nuclei in A375 cells (64.2% ± 2.7 for Dox and 68.8% ± 12.8 for N-Dox) i.e., senescent cells (figure 18.c.). The SA-β-Gal staining was performed to confirm the occurrence of senescence (figure 18.a.). After 48 hours of treatment with 0.45 μM Dox, 0.15 μM N-Dox, it is possible to observe an increase in the number of cells expressing senescent phenotype (blue staining). Treatment with 0.6 $\mu g.mL^{-1}$ of NPC did not significantly increase the SA-β-Gal label (figure 18.d.).

Cancer cells can enter a state of senescence after being exposed to chemotherapeutic agents (ASSARAF et al., 2019; SIKORA et al., 2020) e.g., doxorubicin, which is a potent inducer of senescence in cancer cells (BOJKO et al., 2019). This phenomenon is recognized as a desirable form of treatment for cancer known as therapy-induced senescence (TIS) as it stops the progression of tumors less aggressively (NARDELLA et al., 2011).

The main characteristic that is associated with senescent cells is the loss of proliferative capacity (GORGOULIS et al., 2019). However, it is possible to identify senescent phenotypes with different characteristics e.g., oncogene-induced senescence and stress-induced premature senescence (KUILMAN et al., 2008; TOUSSAINT et al., 2002). The labeling of the lysosomal enzyme SA-β-Gal is a methodology used for detecting senescence in cultured cells (DIMRI et al., 1995) but the expression of genes involved with cell cycle progression e.g., $^{p21Cip1\ /\ WAF1}$ and $p^{16INK4a}$ and with DNA repair, in addition to effective DNA damage, and oxidative stress are variables recurrently measured to detect cell senescence induction (BIELAK-ZMIJEWSKA; MOSIENIAK; SIKORA, 2018).

In addition to the biomarkers mentioned above, the occurrence of polyploidy is a characteristic commonly observed in senescent cancer cells (BESANCENOT et al., 2010). The occurrence of polyploidy is associated with the initial transformation of normal cells into cancerous cells and also is indicative of resistance to treatment and relapse (COWARD; HARDING, 2014). There is evidence of the occurrence of polyploid cells escaping from senescence mechanisms and re-entering the cell cycle after acquiring resistance to drugs or radiation, even so through aberrant buds that manifest cancer stem cell characteristics (SABISZ; SKLADANOWSKI, 2008).

Despite this, there are few studies in which the co-occurrence of senescence and polyploidy has been evaluated (SIKORA et al., 2020). In this sense, several aspects of treatment-induced senescence must be evaluated to identify “scapers” cells associated with tumor recurrence (MOSIENIAK et al., 2015). In the study by Saleh, HCT116 colon-rectal carcinoma and 4T1 breast cancer cells showed phenotypes characteristic of senescent cells e.g., increased size, and SA-β-Gal labeling after doxorubicin treatment and were able to resume proliferation and develop tumors in a murine model (SALEH; TYUTYUNYK-MASSEY; GEWIRTZ, 2019).

The occurrence of tumor recurrence and multiple drug resistance is characterized by resistance to several drugs with different treatment targets (FRANKEN et al., 2006). The clonogenic assay (figure 17.) simulates the effect of long-term treatment and tests the ability of a tumor cell to perform infinite cell divisions, even after exposure to a cytotoxic stimulus (FRANKEN et al., 2006). Our results showed that the treatments with Dox (figure 17.a.) and N-Dox (figura 17.b.) were able to prevent the formation of A375 cell colonies after 14 days of incubation, which indicates that the cells were not able to reverse the damage caused by the formulations, even with a short exposure period. NPC treatment (figure 17.c.) formed colonies as well as control (figure 17.e.).Plating efficiency (PE) and survival fractions are summarized in table 5. Data are expressed as the means of three independent experiments ± SD.

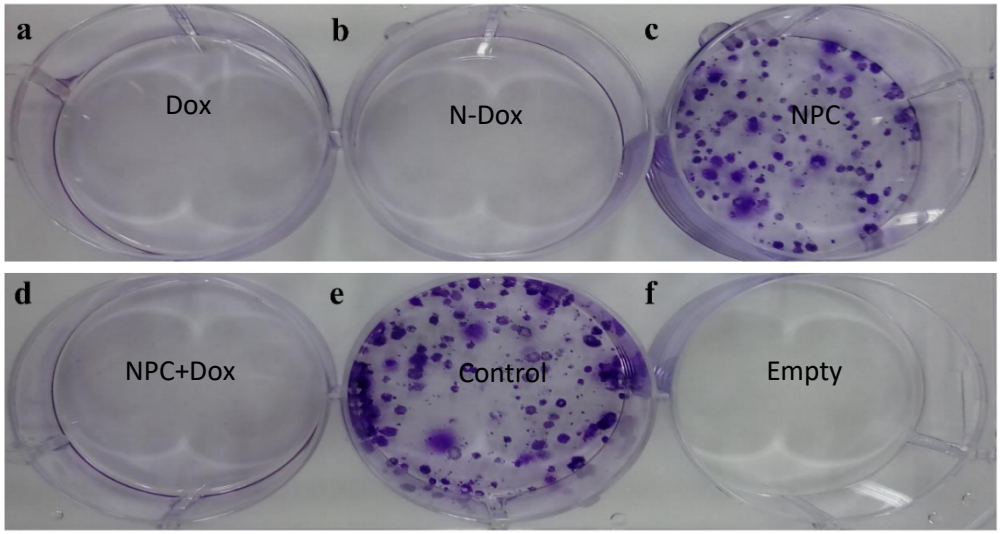

Figure 17. Representative photograph of the clonogenic assay performed in a six-well plate, with clones produced by A-375 cells (a) treatment with 0.45 µM Doxorubicin, (b) treatment with N-DOX 0.13 µM, (c) treatment with NPC 6 $\mu g.ml^{-1}$, (d) treatment with NPC+DOX 2 $\mu g.ml^{-1}$/0.16 µm, (e) untreated cells control with 178 ± 5.03 clones formed after sowing 200 cells, (f) empty well.

Table 5. Number of colonies (NC), plating efficiency (PE), and survival fraction (SF) of A-375 cells after treatment. Data expressed as mean ± S.D. of three independent experiments.

Treatment	NC	PE	SF
DOX	0±0,0	-	0±0,0
N-DOX	0±0,0	-	0±0,0
NPC	156±12,16	-	0,01±0,0
NPC+DOX	0±0,0	-	0±0,0
CC	178±5,03	89,2±2,51	0,01±0,0

Although we observed the occurrence of polyploidy associated with senescence after treatments, the ability to form colonies was completely inhibited (figure 17.) suggesting the absence of cells capable of evading the senescence mechanism since scaper cells are more invasive and form colonies more quickly (MILANOVIC et al., 2018).

From this moment on, the experiments with the NPC + DOX formulation were interrupted by the scarcity of resources.

Oncogenic-induced senescence is a good strategy to stop the development of melanoma (COLLADO et al., 2005). Thus, it is important to investigate the molecular mechanisms involved in the induction of senescence caused by our treatment to recognize which senescent phenotype we are dealing with and find out whether there is the possibility of resistance to treatment.

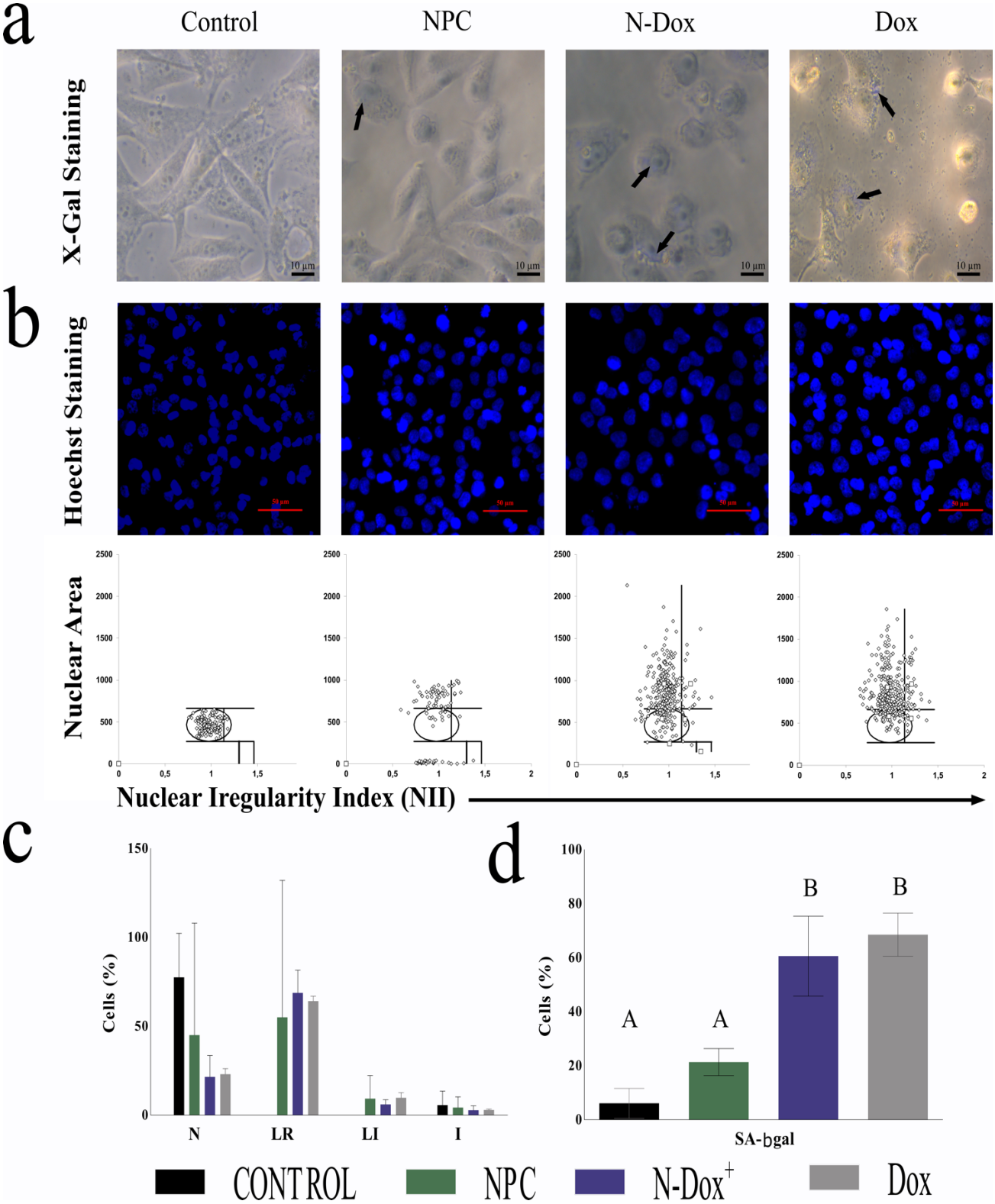

Figure 18. (A) Senescence-associated-β-galactosidase (SA-β-gal) staining of A-375 cells photographed under a phase contrast light microscope; scale bars, 10 μm; magnification 400 x, black arrows indicate positive cells for SA-β-gal (blue staining). (B) Nuclear Morphometric Analysis of A375 cells treated as indicated. Nucleus was stained with Hoechst for confocal microscopy imaging; scale bars, 50 μm;

magnification, 400 x, and have their nuclear area (y-axis) and shape (x-axis) measured.). (C) Nuclei classified as N = normal; I = Irregular; LR = Large Regular, and LI = Large Irregular, showing the percentage of senescent nuclei (LR). (D) Stained levels of SA-β-gal-positive cells. The results were compared by ANOVA and Tukey's mean comparison with a significance level at $p < 0.05$. The letters indicate a significant difference between treatments, n = 6.

4.3. In vitro cardiotoxicity assessment

Undifferentiated H9C2 cells are a classic model of cardiotoxicity (KIMES; BRANDT, 1976) that is accepted for the investigation of heart diseases and toxicity of chemotherapeutic agents such as doxorubicin and resveratrol (GURUSAMY et al., 2010; L'ECUYER et al., 2012).

In addition to understanding the mechanism of action of a candidate for cancer treatment, it is important to conduct studies that help ensure its safety (RICHARD J WEAVER; JEAN-PIERRE VALENTIN, 2018). Doxorubicin induces cardiotoxicity through mechanisms that involve oxidative stress, DNA damage, ferroptosis, and CYP1 disruption (HOEGER; TURISSINI; ASNANI, 2020). Symptoms usually appear after 1 year from treatment, are characterized by chronic dilation of cardiomyocytes and left ventricular dysfunction that leads to cardiac failure (BRODER; GOTTLIEB; LEPOR, 2008). In addition to the clinical symptoms, the number of cardiac progenitor cells is reduced after treatment with Dox (GEISBERG; SAWYER, 2010).

Dox treatment generates significantly higher ROS in H9C2 cells (figure 19.c.), in all concentrations tested, both concerning the control and N-Dox. The treatment with NPC did not cause any significant change concerning the control. Besides, concentrations of 7.2 µM and 1.4 µM from both formulations significantly reduced the viability of cardiac progenitor cells (figure 19.b.). In figure 19.a. we can observe representative photomicrographs of H9C2 cells treated for 48 hours with 7.2 µM of formulations described earlier. The smaller generation of ROS by N-Dox may explain why, despite the potentiation of Dox by the formulation, there was no significant reduction in cell viability compared to Dox, indicating that there is no increase in toxicity to cardiac progenitor cells induced by N-Dox compared to Dox (UPADHYAY; MANTHA; DHIMAN, 2020).

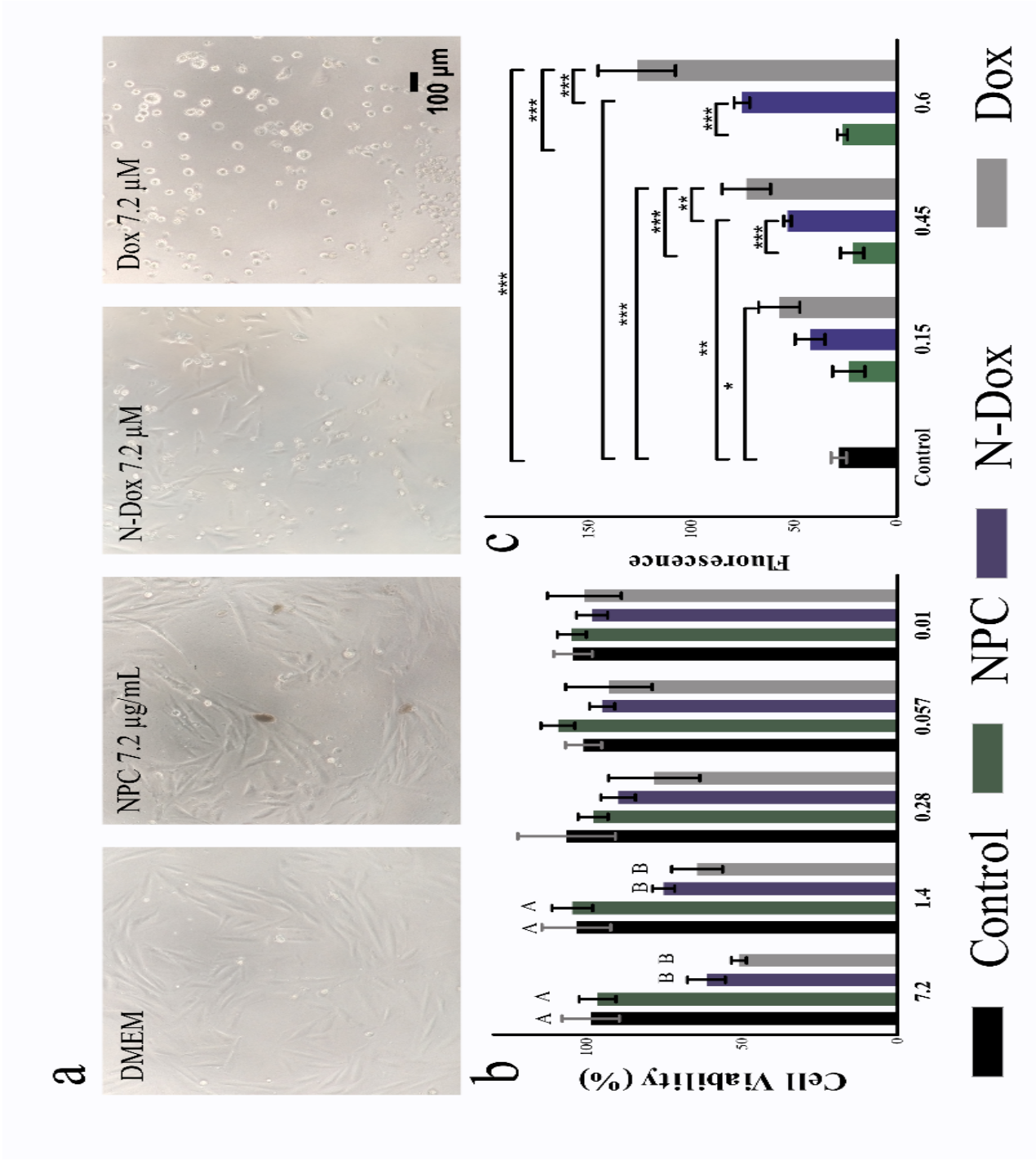

Figure 19. Representative photomicrographs of H9C2 cells treated with dx obtained under a light microscope, scale bars: 100 µm (a); percentage of cell viability after treatments (b), detection of ROS by fluorescence emitted by DCF-DA (c). Concentrations expressed in µM for Dox and N-Dox and in $\mu g.mL^{-1}$ for NPC. The results were compared by ANOVA and Tukey's mean comparison with a significance level at p <0.05. The letters indicate a significant difference between treatments, n = 6.

5. Conclusion

The calcium phosphate nanoparticles (NPC) are shown to be efficient as a drug delivery system for doxorubicin. The system is formed by self-assembly with a retention capacity of 15.77% of the total drug added. The system has a slow release rate, which can provide a longer drug retention time in the circulation. The viability tests demonstrated that the formulations present potentiation of the effect of the drug and reduction of toxicity, mainly in the time of 48 hours of treatment. Functionalization with HA and PEG enhances the effect of the formulation. It has also been shown that the nanoparticles themselves, like HA and PEG, are non-toxic. NPC has shown to be an efficient drug delivery system for Dox. The system is formed by self-assembly with a mean retention capacity of 15.78 % ± 5,33. The system has a slow-release rate, which could provide a longer drug retention time in the circulation. The cell proliferation assays demonstrated that the formulation provided potentiation of the effect of the Dox and reduction of toxicity for human embryonic kidney cells, mainly after 48 hours of treatment. Functionalization with HA and PEG enhances the activity of the formulation. The formulations induced, DNA fragmentation, tetraploidy, and increase in the nuclear area accompanied by increased activity of the enzyme SA-β-Gal which are indicators of the senescent phenotype. Also, no colonies were formed in the long-term survival assay, suggesting the absence of scaper cells. Our preliminary findings suggest that N-Dox has enhanced activity without increasing toxicity to cardiac progenitor cells, which may imply a reduction of cardiopathy incidence. The quantification of the expression of the genes involved with the progression of the cell cycle is fundamental to confirm the hypothesis of no escapers from senescence. This approach will allow that the formulation has its effectiveness and safety assured. The formulation is promising as a potential treatment for melanoma that could reduce damage to patients and reduce treatment costs due to the smaller amount of drug used.

6. References

ABDULELAH, Furqan M.; ALSABAH, Atheer S.; ABDULBAQI, Mustafa R. A Review on Cardio Deleterious Effect of Doxorubicin Therapy with Possible Strategies that may Counteract Cardiotoxicity. **kerbala journal of pharmaceutical sciences**, v. 1, n. 19, 2021.

AGGARWAL, S. K. A histochemical approach to the mechanism of action of cisplatin and its analogues. **Journal of Histochemistry & Cytochemistry**, v. 41, n. 7, p. 1053–1073, 5 jul. 1993.

ALVARENGA, B. M. et al. Nanoparticle phosphate-based composites as vehicles for antimony delivery to macrophages: Possible use in leishmaniasis. **Journal of Materials Chemistry B**, v. 3, n. 48, p. 9250–9259, 2 dez. 2015.

ANDREASSEN, P. R.; MARTINEAU, S. N.; MARGOLIS, R. L. **Chemical induction of mitotic checkpoint override in mammalian cells results in aneuploidy following a transient tetraploid state**. Mutation Research - Fundamental and Molecular Mechanisms of Mutagenesis. **Anais**...Elsevier, 1 dez. 1996. Acesso em: 12 abr. 2020

ARUFFO, A. et al. CD44 is the principal cell surface receptor for hyaluronate. **Cell**, v. 61, n. 7, p. 1303–1313, 29 jun. 1990.

ASCIERTO, P. A. et al. Phase II Trial (BREAK-2) of the BRAF Inhibitor Dabrafenib (GSK2118436) in Patients With Metastatic Melanoma. **J Clin Oncol**, v. 31, p. 3205–3211, 2013.

ASCIERTO, P. A. et al. PP 65 Are GSK2118436 and GSK1120212 effective in melanoma cell lines harboring V600BRAF mutations different from the common V600EBRAF variant? **European Journal of Cancer**, v. 47, p. S11, 1 out. 2011.

ASSARAF, Y. G. et al. The multi-factorial nature of clinical multidrug resistance in cancer. **Drug Resistance Updates**, v. 46, p. 100645, 1 set. 2019.

AZEVEDO, S. J. et al. First-line atezolizumab monotherapy in patients with advanced *BRAF* ^{V600} wild-type melanoma. **Pigment Cell & Melanoma Research**, p. pcmr.12960, 15 fev. 2021.

BAE, Y. H.; PARK, K. **Targeted drug delivery to tumors: Myths, reality and possibilityJournal of Controlled Release**Elsevier B.V., , 10 ago. 2011. . Acesso em: 2 abr. 2020

BARBAULT-FOUCHER, S. et al. Design of poly-ε-caprolactone nanospheres coated with bioadhesive hyaluronic acid for ocular delivery. **Journal of Controlled Release**, v. 83, n. 3, p. 365–375, 30 out. 2002.

BASTIAN, B. C. The Molecular Pathology of Melanoma: An Integrated Taxonomy of Melanocytic Neoplasia. **Annual Review of Pathology: Mechanisms of Disease**, v. 9, n. 1, p. 239–271, 24 jan. 2014.

BERWICK, M. et al. Melanoma epidemiology and prevention. In: **Cancer Treatment and Research**. [s.l.] Kluwer Academic Publishers, 2016. v. 167p. 17–49.

BESANCENOT, R. et al. A Senescence-Like Cell-Cycle Arrest Occurs During Megakaryocytic Maturation: Implications for Physiological and Pathological Megakaryocytic Proliferation. **PLoS Biology**, v. 8, n. 9, p. e1000476, 7 set. 2010.

BIELAK-ZMIJEWSKA, A.; MOSIENIAK, G.; SIKORA, E. **Is DNA damage indispensable for stress-induced senescence?Mechanisms of Ageing and Development**Elsevier Ireland Ltd, , 1 mar. 2018. . Acesso em: 28 fev. 2021

BOJKO, A. et al. Diversity of the Senescence Phenotype of Cancer Cells Treated with Chemotherapeutic Agents. **Cells**, v. 8, n. 12, p. 1501, 23 nov. 2019.

BORATTO, F. A. et al. Alpha-tocopheryl succinate improves encapsulation, pH-sensitivity, antitumor activity and reduces toxicity of doxorubicin-loaded liposomes. **European Journal of Pharmaceutical Sciences**, v. 144, p. 105205, 1 mar. 2020.

BORTNER, C. D.; OLDENBURG, N. B. E.; CIDLOWSKI, J. A. **The role of DNA fragmentation in apoptosisTrends in Cell Biology**Elsevier, , 1 jan. 1995. . Acesso em: 14 abr. 2020

BRODER, H.; GOTTLIEB, R. A.; LEPOR, N. E. **Chemotherapy and cardiotoxicityReviews in Cardiovascular Medicine**NIH Public Access, , mar. 2008. Disponível em: </pmc/articles/PMC3723407/>. Acesso em: 28 fev. 2021

CEZAR, G. G. **Can human embryonic stem cells contribute to the discovery of safer and more effective drugs?Current Opinion in Chemical Biology**Elsevier Current Trends, , 1 ago. 2007. . Acesso em: 9 abr. 2020

CHATTERJEE, K. et al. Doxorubicin Cardiomyopathy. **Cardiology**, v. 115, n. 2, p. 155–162, jan. 2010.

CHUANG, C.-H. et al. Discovery of Akt Kinase Inhibitors through Structure-Based Virtual Screening and Their Evaluation as Potential Anticancer Agents. **International Journal of Molecular Sciences**, v. 16, n. 2, p. 3202–3212, 2 fev. 2015.

COLLADO, M. et al. Tumour biology: Senescence in premalignant tumours. **Nature**, v. 436, n. 7051, p. 642, 4 ago. 2005.

COWARD, J.; HARDING, A. Size does matter: Why polyploid tumor cells are critical drug targets in the war on cancer. **Frontiers in Oncology**, v. 4 MAY, p. 123, 26 maio 2014.

DEBACQ-CHAINIAUX, F. et al. Protocols to detect senescence-associated beta-galactosidase (SA-βgal) activity, a biomarker of senescent cells in culture and in vivo. **Nature Protocols**, v. 4, n. 12, p. 1798–1806, 19 nov. 2009.

DIETRICH, A. et al. High CD44 surface expression on primary tumours of malignant melanoma correlates with increased metastatic risk and reduced survival. **European Journal of Cancer Part A**, v. 33, n. 6, p. 926–930, 1 maio 1997.

DIMRI, G. P. et al. A biomarker that identifies senescent human cells in culture and in aging skin in vivo. **Proceedings of the National Academy of Sciences of the United States of America**, v. 92, n. 20, p. 9363–9367, 26 set. 1995.

FAHMY, T. M. et al. Targeted for drug delivery. **Materials Today**, v. 8, n. 8 SUPPL., p. 18–26, 1 ago. 2005.

FATTORE, L. et al. **MicroRNAs in melanoma development and resistance to target therapyOncotarget**Impact Journals LLC, , 2017. Disponível em: </pmc/articles/PMC5400662/>. Acesso em: 28 fev. 2021

FICHTINGER-SCHEPMAN, A. M. J. et al. In Vivo Cis-Diamminedichloroplatinum(II)-DNA Adduct Formation and Removal as Measured with Immunochemical Techniques. In: **Platinum and Other Metal Coordination Compounds in Cancer Chemotherapy**. [s.l.] Springer US, 1988. p. 32–46.

FILIPPI-CHIELA, E. C. et al. Autophagy interplay with apoptosis and cell cycle regulation in the growth inhibiting effect of resveratrol in glioma cells. **PLoS ONE**, v. 6, n. 6, 2011.

FILIPPI-CHIELA, E. C. et al. Nuclear Morphometric Analysis (NMA): Screening of Senescence, Apoptosis and Nuclear Irregularities. **PLoS ONE**, v. 7, n. 8, p. e42522, 8 ago. 2012.

FLOREA, Ana-Maria; BÜSSELBERG, Dietrich. Cisplatin as an anti-tumor drug: cellular mechanisms of activity, drug resistance and induced side effects. **Cancers**, v. 3, n. 1, p. 1351-1371, 2011.

FRANKEN, N. A. P. et al. Clonogenic assay of cells in vitro. **Nature Protocols**, v. 1, n. 5, p. 2315–2319, 21 dez. 2006.

FUERTES, M. A. et al. Cisplatin biochemical mechanism of action: from cytotoxicity to induction of cell death through interconnections between apoptotic and necrotic pathways. **Current medicinal chemistry**, v. 10, n. 3, p. 257-266, 2003.

FUERTES, M. et al. Cisplatin Biochemical Mechanism of Action: From Cytotoxicity to Induction of Cell Death Through Interconnections Between Apoptotic and Necrotic Pathways. **Current Medicinal Chemistry**, v. 10, n. 3, p. 257–266, 26 ago. 2012.

GEISBERG, C. A.; SAWYER, D. B. **Mechanisms of anthracycline cardiotoxicity and strategies to decrease cardiac damageCurrent Hypertension Reports**NIH Public Access, , dez. 2010. Disponível em: </pmc/articles/PMC3999517/>. Acesso em: 28 fev. 2021

GOH, J. Y. et al. Development and use of in vitro alternatives to animal testing by the pharmaceutical industry 1980-2013. **Toxicology Research**, v. 4, n. 5, p. 1297–1307, 27 jun. 2015.

GORGOULIS, V. et al. **Cellular Senescence: Defining a Path ForwardCell**Cell Press, , 31 out. 2019. . Acesso em: 28 fev. 2021

GOUSSETIS, D. J. et al. Autophagy is a critical mechanism for the induction of the antileukemic effects of arsenic trioxide. **Journal of Biological Chemistry**, v. 285, n. 39, p. 29989–29997, 24 set. 2010.

GURUSAMY, N. et al. Cardioprotection by resveratrol: a novel mechanism via autophagy involving the mTORC2 pathway. **Cardiovascular Research**, v. 86, n. 1, p. 103–112, 1 abr. 2010.

GÜVEN, K. et al. Cisplatin and carboplatin combination as second-line chemoth... : Melanoma Research. **Melanoma Research**, v. 11, n. 4, p. 411–415, ago. 2001.

HALEY, B.; FRENKEL, E. **Nanoparticles for drug delivery in cancer treatmentUrologic Oncology: Seminars and Original Investigations**, jan. 2008. . Acesso em: 2 abr. 2020

HANUSOVA, V. et al. Potential Anti-cancer Drugs Commonly Used for Other Indications. v. 15, n. 1, p. 35–52, 2015.

HAUSCHILD, A. et al. Dabrafenib in BRAF-mutated metastatic melanoma: A multicentre, open-label, phase 3 randomised controlled trial. **The Lancet**, v. 380, n. 9839, p. 358–365, 28 jul. 2012.

HOEGER, C. W.; TURISSINI, C.; ASNANI, A. **Doxorubicin Cardiotoxicity: Pathophysiology UpdatesCurrent Treatment Options in Cardiovascular Medicine**Springer, , 1 nov. 2020. Disponível em: <https://link.springer.com/article/10.1007/s11936-020-00842-w>. Acesso em: 28 fev. 2021

HOFFMAN, A. S. **The origins and evolution of "controlled" drug delivery systemsJournal of Controlled Release**Elsevier, , 18 dez. 2008. . Acesso em: 2 abr. 2020

HUANG, Dong et al. Nanodrug delivery systems modulate tumor vessels to increase the enhanced permeability and retention effect. **Journal of Personalized Medicine**, v. 11, n. 2, p. 124, 2021.

HUTCHINSON, Katherine E. et al. BRAF fusions define a distinct molecular subset of melanomas with potential sensitivity to MEK inhibition. **Clinical Cancer Research**, v. 19, n. 24, p. 6696-6702, 2013.

INCA. **Tipos de câncer | INCA - Instituto Nacional de Câncer**. Disponível em: <https://www.inca.gov.br/tipos-de-cancer/cancer-de-pele-melanoma>. Acesso em: 14 abr. 2020.

IYER, A. K. et al. **Exploiting the enhanced permeability and retention effect for tumor targetingDrug Discovery Today**Elsevier Current Trends, , 1 set. 2006. . Acesso em: 5 abr. 2020

KAROUSOU, E. et al. **Roles and targeting of the HAS/hyaluronan/CD44 molecular system in cancerMatrix Biology**Elsevier B.V., , 1 maio 2017. . Acesso em: 12 abr. 2020

KIMES, B. W.; BRANDT, B. L. Properties of a clonal muscle cell line from rat heart. **Experimental Cell Research**, v. 98, n. 2, p. 367–381, 15 mar. 1976.

KOSMULSKI, M. pH-dependent surface charging and points of zero charge. IV. Update and new approach. **Journal of Colloid and Interface Science**, v. 337, n. 2, p. 439–448, 15 set. 2009.

KUILMAN, T. et al. Oncogene-Induced Senescence Relayed by an Interleukin-Dependent Inflammatory Network. **Cell**, v. 133, n. 6, p. 1019–1031, 13 jun. 2008.

L'ECUYER, T. J. et al. Effect of hypothermia on doxorubicin-induced cardiac myoblast signaling and cell death. **Cardiovascular Pathology**, v. 21, n. 2, p. 96–104, 1 mar. 2012.

LANGER, K. et al. Optimization of the preparation process for human serum albumin (HSA) nanoparticles. **International Journal of Pharmaceutics**, v. 257, n. 1–2, p. 169–180, 12 maio 2003.

LARKIN, J. et al. Combined nivolumab and ipilimumab or monotherapy in untreated Melanoma. **New England Journal of Medicine**, v. 373, n. 1, p. 23–34, 2 jul. 2015.

LIU, X. et al. Enhanced retention and cellular uptake of nanoparticles in tumors by controlling their aggregation behavior. **ACS Nano**, v. 7, n. 7, p. 6244–6257, 23 jul. 2013.

LONG, G. V. et al. Increased MAPK reactivation in early resistance to dabrafenib/trametinib combination therapy of BRAF-mutant metastatic melanoma. **Nature Communications**, v. 5, n. 1, p. 1–9, 2 dez. 2014.

MANSOUR, A. M. et al. A new approach for the treatment of malignant melanoma: Enhanced antitumor efficacy of an albumin-binding doxorubicin prodrug that is cleaved by matrix metalloproteinase 2. **Cancer Research**, v. 63, n. 14, p. 4062–4066, 15 jul. 2003.

MENKE, A. et al. Formation of Cisplatin Adducts with the Epigenetically Relevant Nucleobase 5-Methylcytosine. **European Journal of Inorganic Chemistry**, v. 2021, n. 1, p. 30–36, 8 jan. 2021.

MILANOVIC, M. et al. Senescence-associated reprogramming promotes cancer stemness. **Nature**, v. 553, n. 7686, p. 96–100, 4 jan. 2018.

MOLINARO, R. et al. Leukocyte-mimicking nanovesicles for effective doxorubicin delivery to treat breast cancer and melanoma. **Biomaterials Science**, v. 8, n. 1, p. 333–341, 1 jan. 2020.

MOLLATAGHI, A. **Bioactive compounds from the Bark of Beilschmiedia Palembanica (Miq.) Kosterm Phytochemistry View project Bioactive compounds from the Bark of Beilschmiedia Palembanica (Miq.) Kosterm View project Bioactive compounds from the Bark of Beilschmiedia Palembanica (Miq.) KostermBasic Research Journal of Microbiology**. [s.l: s.n.]. . Acesso em: 7 abr. 2020.

MOSIENIAK, G. et al. Polyploidy Formation in Doxorubicin-Treated Cancer Cells Can Favor Escape from Senescence. **Neoplasia (United States)**, v. 17, n. 12, p. 882–893, 1 dez. 2015.

MULLER, C. et al. Cellular pharmacokinetics of doxorubicin in patients with chronic lymphocytic leukemia: comparison of bolus administration and continuous infusion. **Cancer Chemotherapy and Pharmacology**, v. 32, n. 5, p. 379–384, set. 1993.

NARDELLA, C. et al. **Pro-senescence therapy for cancer treatmentNature Reviews Cancer**Nature Publishing Group, , 24 jul. 2011. Disponível em: <www.nature.com/reviews/cancer>. Acesso em: 28 fev. 2021

O'BRIEN, J. et al. Investigation of the Alamar Blue (resazurin) fluorescent dye for the assessment of mammalian cell cytotoxicity. **European Journal of Biochemistry**, v. 267, n. 17, p. 5421–5426, 1 set. 2000.

PANDEY, S. D. et al. Structural and elemental analysis of biochars in the search of a synthetic path to mimetize anthropic Amazon soils. **Journal of Environmental Management**, v. 279, p. 111685, 15 jan. 2021.

PATIL, S. et al. Protein adsorption and cellular uptake of cerium oxide nanoparticles as a function of zeta potential. **Biomaterials**, v. 28, n. 31, p. 4600–4607, 1 nov. 2007.

PEER, D. et al. **Nanocarriers as an emerging platform for cancer therapyNature Nanotechnology**Nature Publishing Group, , dez. 2007. Disponível em: <https://www.nature.com/articles/nnano.2007.387>. Acesso em: 6 mar. 2021

PINAR, N. et al. Protective effect of dexpanthenol on cisplatin induced nephrotoxicity in rats. **Biotechnic & Histochemistry**, p. 1–5, 26 fev. 2021.

RICCARDI, C.; NICOLETTI, I. Analysis of apoptosis by propidium iodide staining and flow cytometry. **Nature Protocols**, v. 1, n. 3, p. 1458–1461, 9 ago. 2006.

RICHARD J WEAVER; JEAN-PIERRE VALENTIN. Today's Challenges to De-Risk and Predict Drug Safety in Human "Mind-the-Gap." **Toxicological Sciences**, v. 167, n. 2, p. 307–321, 29 out. 2018.

ROMANO, M. F. et al. Rapamycin inhibits doxorubicin-induced NF-κB/Rel nuclear activity and enhances the apoptosis of melanoma cells. **European Journal of Cancer**, v. 40, n. 18, p. 2829–2836, 1 dez. 2004.

ROMANO, S. et al. Synergy between enzastaurin doxorubicin in inducing melanoma apoptosis. **Pigment Cell & Melanoma Research**, v. 26, n. 6, p. 900–911, 1 nov. 2013.

RUENRAROENGSAK, P.; COOK, J. M.; FLORENCE, A. T. **Nanosystem drug targeting: Facing up to complex realitiesJournal of Controlled Release**Elsevier, , 15 fev. 2010. . Acesso em: 2 abr. 2020

SABISZ, M.; SKLADANOWSKI, A. Cancer stem cells and escape from drug-induced premature senescence in human lung tumor cells: Implications for drug resistance and in vitro drug screening models. **Cell Cycle**, v. 8, n. 19, p. 3208–3217, 1 out. 2009.

SABISZ, M.; SKLADANOWSKI, A. Modulation of Cellular Response to Anticancer Treatment by Caffeine: Inhibition of Cell Cycle Checkpoints, DNA Repair and More. **Current Pharmaceutical Biotechnology**, v. 9, n. 4, p. 325–336, 3 ago. 2008.

SALEH, T.; TYUTYUNYK-MASSEY, L.; GEWIRTZ, D. A. Tumor cell escape from therapy-induced senescence as a model of disease recurrence after dormancy. **Cancer Research**, v. 79, n. 6, p. 1044–1046, 15 mar. 2019.

SCHADENDORF, D. et al. Melanoma. **Nature Reviews Disease Primers**, v. 1, n. 1, p. 1–20, 23 abr. 2015.

SHEN, H. et al. Coating solid lipid nanoparticles with hyaluronic acid enhances antitumor activity against melanoma stem-like cells. **Theranostics**, v. 5, n. 7, p. 755–771, 2015.

SIEGEL, R. L. et al. Cancer Statistics, 2021. **CA: A Cancer Journal for Clinicians**, v. 71, n. 1, p. 7–33, 12 jan. 2021.

Siegel, R. L., Miller, K. D., Goding Sauer, A., Fedewa, S. A., Butterly, L. F., Anderson, J. C., ... & Jemal, A. (2020). Colorectal cancer statistics, 2020. *CA: a cancer journal for clinicians*, *70*(3), 145-164.
SIEGEL, R. L.; MILLER, K. D.; JEMAL, A. Cancer statistics, 2020. **CA: A Cancer Journal for Clinicians**, v. 70, n. 1, p. 7–30, 8 jan. 2020.

SIKORA, E. et al. **Therapy-induced polyploidization and senescence: Coincidence or interconnection?Seminars in Cancer Biology**Academic Press, , 1 dez. 2020. . Acesso em: 28 fev. 2021

SUO, Z.; LIPPARD, S. J.; JOHNSON, K. A. Single d(GpG)/cis-diammineplatinum(II) adduct-induced inhibition of DNA polymerization. **Biochemistry**, v. 38, n. 2, p. 715–726, 12 jan. 1999.

SYED, M.; SKONBERG, C.; HANSEN, S. H. Effect of some organic solvents on oxidative phosphorylation in rat liver mitochondria: Choice of organic solvents. **Toxicology in Vitro**, v. 27, n. 8, p. 2135–2141, 1 dez. 2013.

TABAKOVIĆ, A.; KESTER, M.; ADAIR, J. H. Calcium phosphate-based composite nanoparticles in bioimaging and therapeutic delivery applications. **Wiley Interdisciplinary Reviews: Nanomedicine and Nanobiotechnology**, v. 4, n. 1, p. 96–112, 1 jan. 2012.

TANGELLA, Lokeswari P.; CLARK, Michael E.; GRAY, Elin S. Resistance mechanisms to targeted therapy in BRAF-mutant melanoma-A mini review. **Biochimica et Biophysica Acta (BBA)-General Subjects**, v. 1865, n. 1, p. 129736, 2021.

TEYMOURI, M. et al. Investigation of Hexadecylphosphocholine (miltefosine) usage in Pegylated liposomal doxorubicin as a synergistic ingredient: In vitro and in vivo evaluation in mice bearing C26

colon carcinoma and B16F0 melanoma. **European Journal of Pharmaceutical Sciences**, v. 80, p. 66–73, 20 ago. 2015.

THOMÉ, M. P. et al. Ratiometric analysis of Acridine Orange staining in the study of acidic organelles and autophagy. **Journal of Cell Science**, v. 129, n. 24, p. 4622–4632, 15 dez. 2016.

THORN, C. F. et al. Doxorubicin pathways: Pharmacodynamics and adverse effects. **Pharmacogenetics and Genomics**, v. 21, n. 7, p. 440–446, jul. 2011.

TONELLI, F. M. P. et al. Functionalized nanomaterials: Are they effective to perform gene delivery to difficult-to-transfect cells with no cytotoxicity? **Nanoscale**, v. 7, n. 43, p. 18036–18043, 21 nov. 2015.

TÓTARO, P. I. S. **Application of multifunctional nanoparticles based on calcium phosphate as a platform for imaging and treatment of breast cancer in vitro**. Belo Horizonte: [s.n.].

TOUSSAINT, O. et al. Stress-induced premature senescence and tissue ageing. **Biochemical Pharmacology**, v. 64, n. 5–6, p. 1007–1009, 1 set. 2002.

UPADHYAY, S.; MANTHA, A. K.; DHIMAN, M. Glycyrrhiza glabra (Licorice) root extract attenuates doxorubicin-induced cardiotoxicity via alleviating oxidative stress and stabilising the cardiac health in H9c2 cardiomyocytes. **Journal of Ethnopharmacology**, v. 258, p. 112690, 10 ago. 2020.

VICHAI, V.; KIRTIKARA, K. Sulforhodamine B colorimetric assay for cytotoxicity screening. **Nature Protocols**, v. 1, n. 3, p. 1112–1116, 17 ago. 2006.

WILSON, M. A.; SCHUCHTER, L. M. Chemotherapy for melanoma. In: **Cancer Treatment and Research**. [s.l.] Kluwer Academic Publishers, 2016. v. 167p. 209–229.

WU, D.; YOTNDA, P. Production and detection of reactive oxygen species (ROS) in cancers. **Journal of Visualized Experiments**, n. 57, p. 3357, 2011.

XIAO, Shuo et al. Doxorubicin has dose-dependent toxicity on mouse ovarian follicle development, hormone secretion, and oocyte maturation. **Toxicological Sciences**, v. 157, n. 2, p. 320-329, 2017.

YONCHEVA, K. et al. Optimization and in-vitro/in-vivo evaluation of doxorubicin-loaded chitosan-alginate nanoparticles using a melanoma mouse model. **International Journal of Pharmaceutics**, v. 556, p. 1–8, 10 fev. 2019.

ZHANG, L. et al. Doxorubicin-loaded polypeptide nanorods based on electrostatic interactions for cancer therapy. **Journal of Colloid and Interface Science**, v. 464, p. 126–136, 15 fev. 2016.

ZHANG, M. et al. Co-delivery of Etoposide and Cisplatin in Dual Drug Loaded Nanoparticles Synergistically Improves Chemoradiotherapy in Non-Small Cell Lung Cancer Models. **Acta Biomaterialia**, 5 fev. 2021.

ZHANG, X.; TEODORO, J. G.; NADEAU, J. L. Intratumoral gold-doxorubicin is effective in treating melanoma in mice. **Nanomedicine: Nanotechnology, Biology, and Medicine**, v. 11, n. 6, p. 1365–1375, 1 ago. 2015.

ZHANG, Y.; KOHLER, N.; ZHANG, M. Surface modification of superparamagnetic magnetite nanoparticles and their intracellular uptake. **Biomaterials**, v. 23, n. 7, p. 1553–1561, 1 abr. 2002.